Supporting Information

Molecular engineering of gCN-based multifunctional photocatalysts via in situ covalent modification

Zhenxing Li[#], Hong Tu[#], Taihong Zhang, Jinhong Hu, Xiang Zhou, Liwei Liu, Jian Wu*, Song Yang*

State Key Laboratory of Green Pesticide, Key Laboratory of Green Pesticide and Agricultural Bioengineering, Ministry of Education, Center for R&D of Fine Chemicals of Guizhou University, Guiyang, 550025, China

[#] The two authors contribute equally to this work.

* Corresponding author.
E-mail: jhzx.msm@gmail.com or syang@gzu.edu.cn (S. Yang); jwu6@gzu.edu.cn (J. Wu).

Contents

1. General procedure of antibacterial and pot experiment……..……...……....3
2. Chemical structure of materials and organic pollutants.……..…….....3
3. Organic pollutants degradation and materials characterization…….…...…….....4
4. Material reusability…...…….……11
5. High resolution of tetracycline degradation intermediates…….…13
6. Mineralization assay…….…..……...…..…….....19
7. Electron-hole calculation…….……..…….....20
8. ROS observation……..……..…….....…....24
9. Pesticide degradation plant toxicity test……...…….…..…….……..25
10. Relevant Tables…….……...…...…....27
11. References……..……....…33

1. Multifunctional investigation of catalysts

1.1. Antibacterial test of catalyst

To explore the wide application of the prepared catalyst, their inhibitory activity against bacteria *Xoo*, *Psa*, *Xac* was also evaluated. Briefly, catalyst gCN or GCN-X (2 mg) was added to a medium (5 mL) containing bacteria (OD_{595} = 0.6) and photoreacted for 30 min under visible light irradiation. Then it was cultured in a shaker (28 ℃, 220 rmp) for 24-36 h, and the corresponding inhibition rate was calculated by turbidity method. The damage of reactive oxygen species (ROS) produced by catalyst on the bacteria morphology was observed by TEM (JEM-2100F, Japan). The corresponding ROS detection is achieved by a Fluoromax-4 cP fluorescence spectrophotometer (HORIBA Scientific, Irvine, CA, U.S.A.).[1,2]

1.2. Pesticide degradation plant toxicity test

Based on pot experiment, the degradation behavior of commercial pesticides (Paraquat, Ningnanmycin and Bismerthiazol) by gCN-A and the toxicity of degradation products to plants were simulated. The pesticide concentration was changed to 50 mg/L, the light (450 nm, 12 W) duration was changed to 30 min, and other experimental procedures were the same as before.

2. Chemical structure of organic pollutants and materials

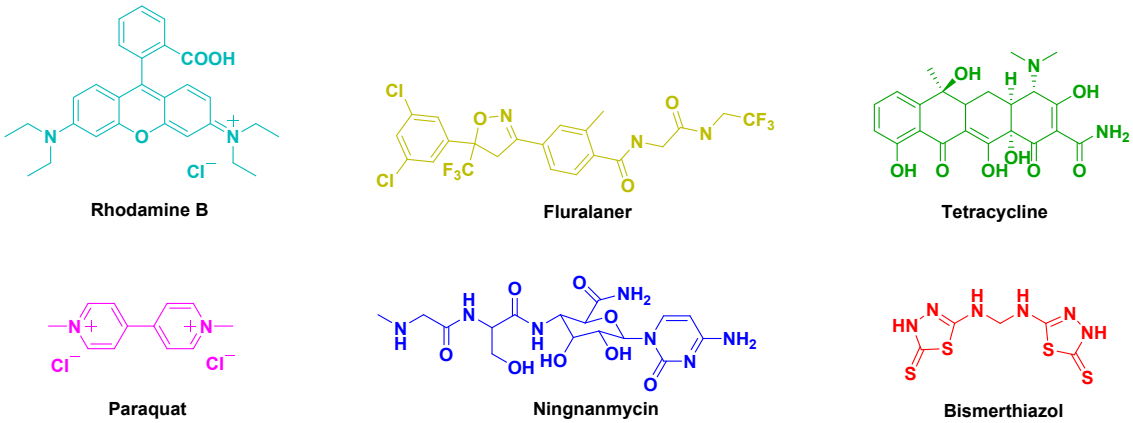

Fig. S1. Chemical structure of organic pollutants used for degradation.

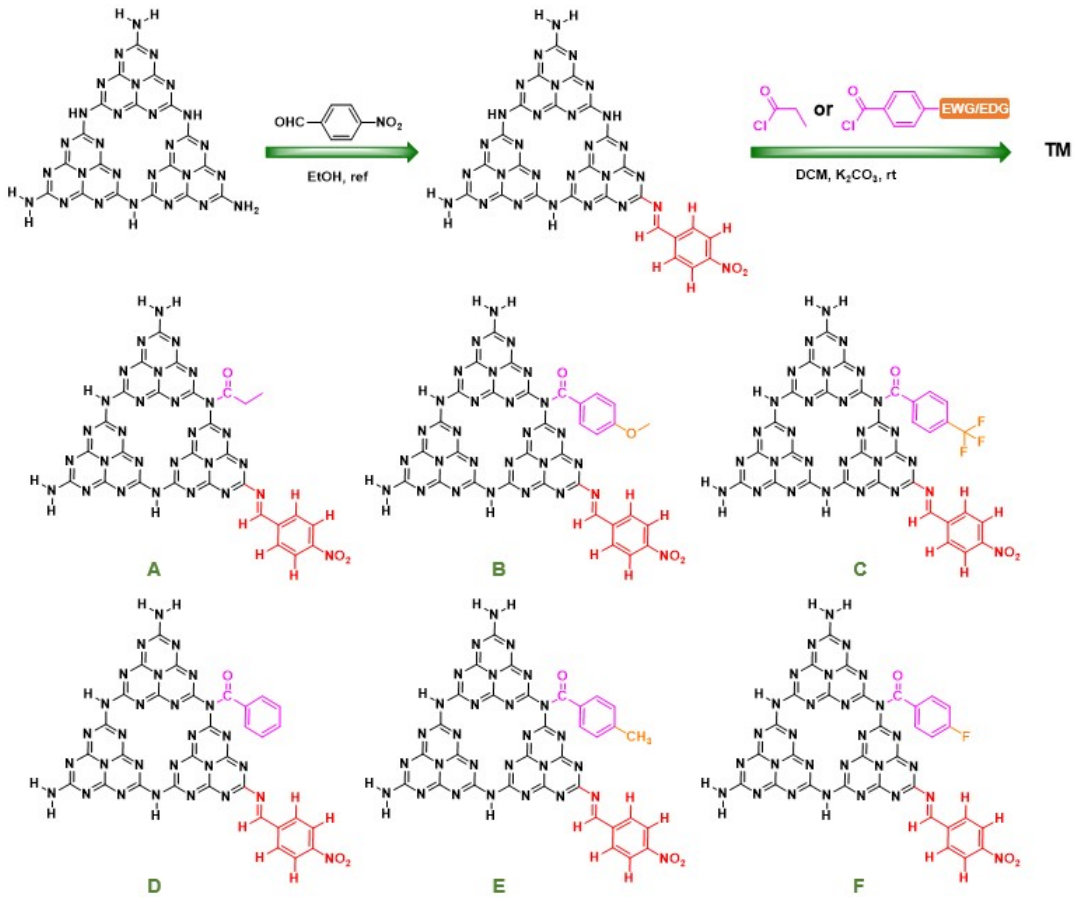

Fig. S2. Preparation of target materials. Chemical preparation process of the target material. A-F represents the chemical unit building structure of materials gCN-A to gCN-F, respectively.

3. Organic pollutants degradation and materials characterization

3.1. Degradation effect of materials on RhB

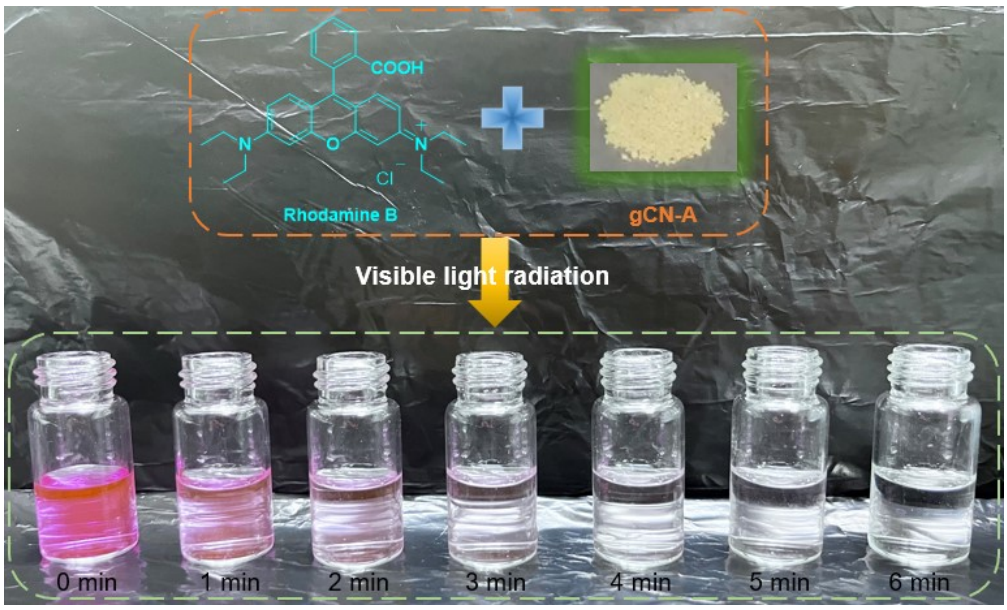

Fig. S3. Colour change of RhB solution containing gCN-A under visible light radiation at different times.

3.2. Photoluminescence (PL) analysis

Briefly, the parent gCN or catalyst gCN-X powder (2 mg) was dissolved in distilled water (2 mL) and ultrasonicated in a microwave cell for 15 min. Subsequently, the corresponding sample tubes were taken out and allowed to stand for 5 min, and the suspensions (1 mL) were respectively sucked for PL detection using a HORIBA Fluorolog-QM spectrometer (Canada) at 360 nm (scan speed: 1200 nm/min; PMT voltage: 700 V; slit: 5.0 nm). All testing conditions remained consistent within the same batch, with the optimization function turned off.

3.3. BET surface comparison

Since the chemical structure of gCN-B/E and gCN-C/F is highly similar, we supplement the BET of gCN-B and gCN-C and find that there is also a similar trend of larger specific surface area. The BET value of gCN-580 is between gCN and gCN-X, as shown in Table S1 and Fig. S4.

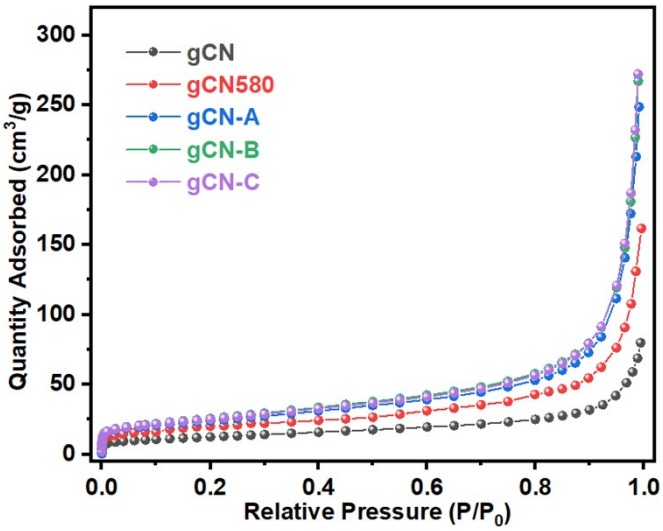

Fig. S4. The nitrogen adsorption–desorption isotherms of gCN, gCN580, gCN-A, gCN-B and gCN-C.

3.4. DLS experiments

Since the parent gCN and the prepared catalyst gCN-X are slightly soluble in water, the dispersion and dispersion stability of the material in water were not initially investigated. Here, we supplemented dynamic light scattering (DLS) experiments to measure particle size distributions at different time points to assess the dispersion and stability of catalysts in water. The DLS test results of gCN, gCN580 and gCN-X are shown in Fig. S5-S6. The particle size distribution of the catalyst before and after modification changes significantly, and the average particle size of the suspension is sorted as follows: gCN (986.80 nm) > gCN580 (861.09 nm) > gCN-A (565.39 nm) > gCN-D (555.86 nm) > gCN-B (482.82 nm) > gCN-C (311.03 nm). This indicates that the surface modification of hydrophobic chemical groups may improve the dispersion of gCN-X catalyst in water, making the originally large catalyst particles more uniformly dispersed. In addition, gCN-X showed a smaller particle size in water, further indicating improved dispersion. This improvement may allow the catalyst to remain in good suspension for a long time, reducing the risk of sedimentation or aggregation. As a result, the dispersion of the modified material in water is significantly improved.

In order to further investigate the dispersion stability of the catalyst suspension, we placed the catalyst suspension at room temperature for 72 hours and found that no sedimentation or aggregation occurred. The particle size distribution and average

particle size of the catalysts after 0 hours and 72 hours showed that they did not produce significant changes, and maintained high dispersion stability in aqueous solution (Fig. S7).

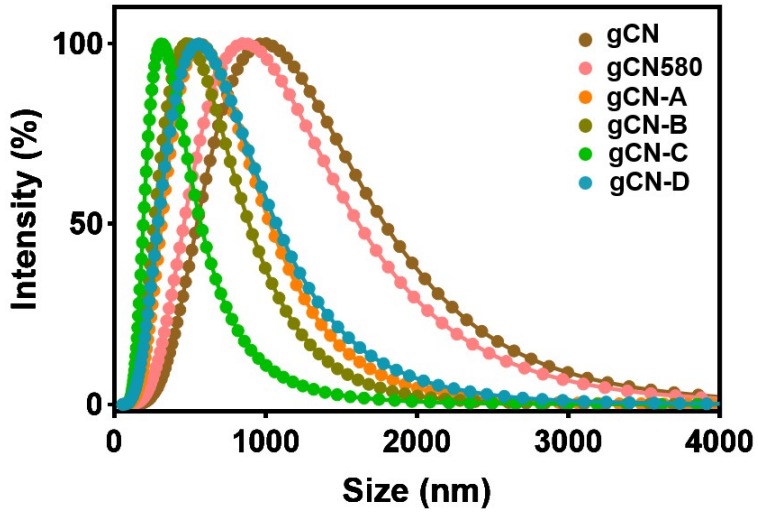

Fig. S5. Comparison of particle size distribution of different materials in water.

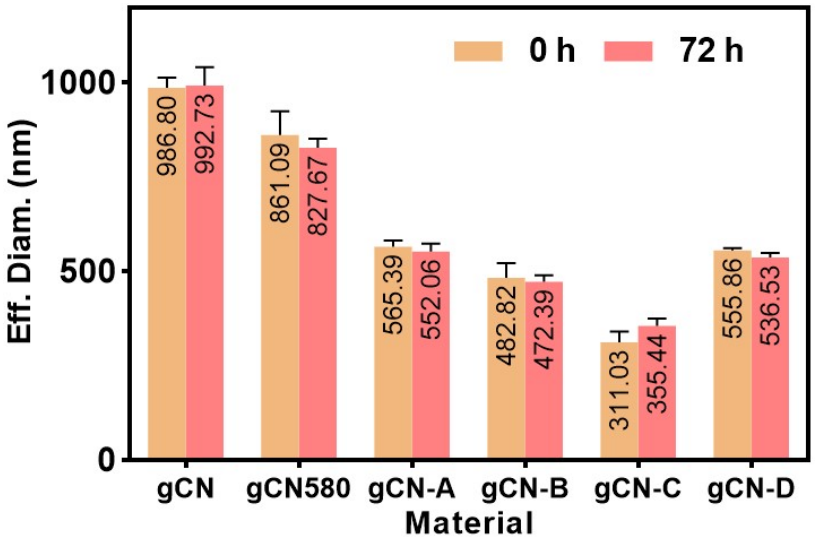

Fig. S6. Comparison of average particle size of materials in water at 0 h and 72 h.

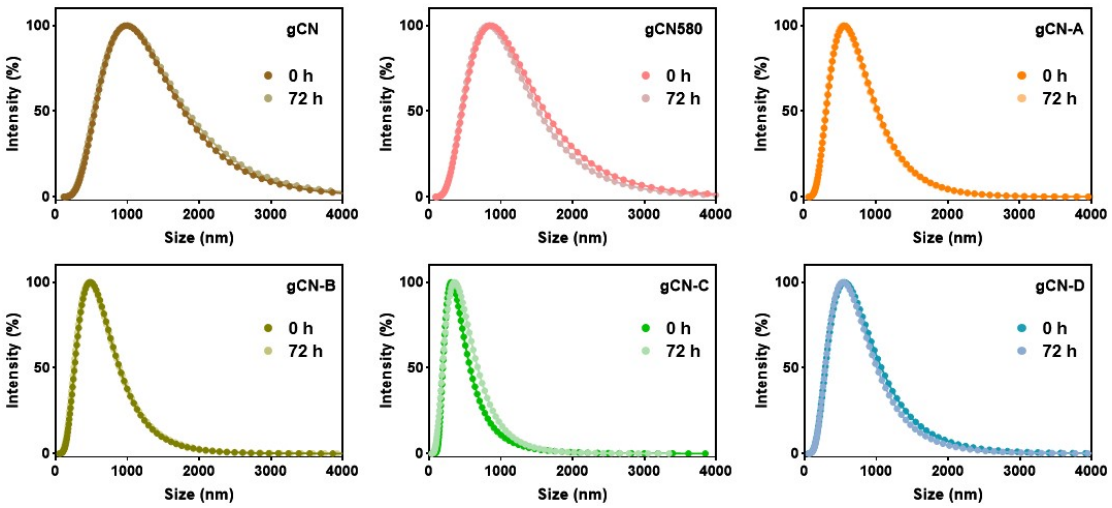

Fig. S7. Comparison of particle size distribution of the same material in water at 0 h and 72 h.

3.5. TGA experiments

The TGA of gCN, gCN-A and gCN-C (Fig. S8) analysis indicates that the initial decomposition temperatures of the three materials are all around 600 °C. Among them, gCN-A exhibits the highest mass loss percentage (97.51%) and thermal stability (729.41 °C), while the parent gCN has the lowest thermal stability (696.98 °C) and mass loss percentage (94.36%). This indicates that the introduction of chemical groups has improved the thermal stability of gCN-X.

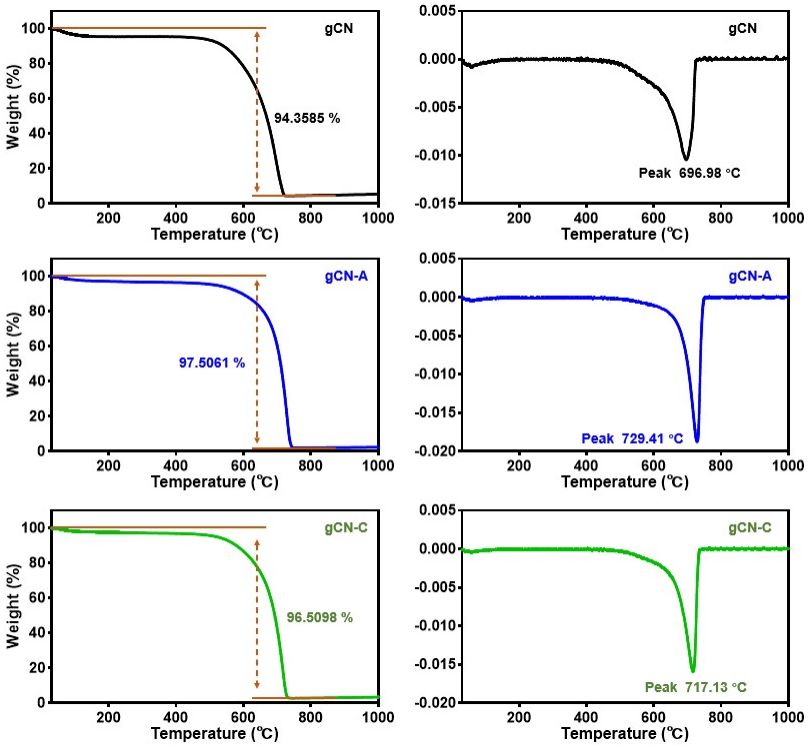

Fig. S8. Thermogravimetric analysis comparison of materials gCN, gCN-A, and gCN-C.

3.6. Electrochemical properties

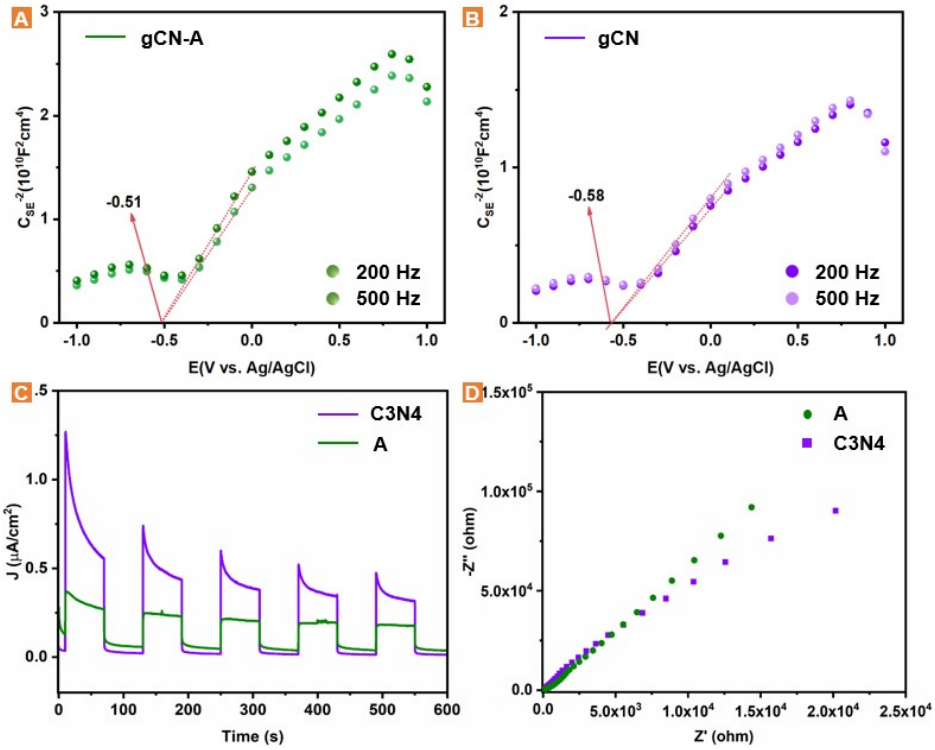

Fig. S9. Mott-Schottky plots of gCN (A) and gCN-A (B) at 200 and 500 Hz. Transient photocurrent (C) and EIS Nyquist plots (D) of gCN and gCN-A.

3.7. Time-resolved PL spectra

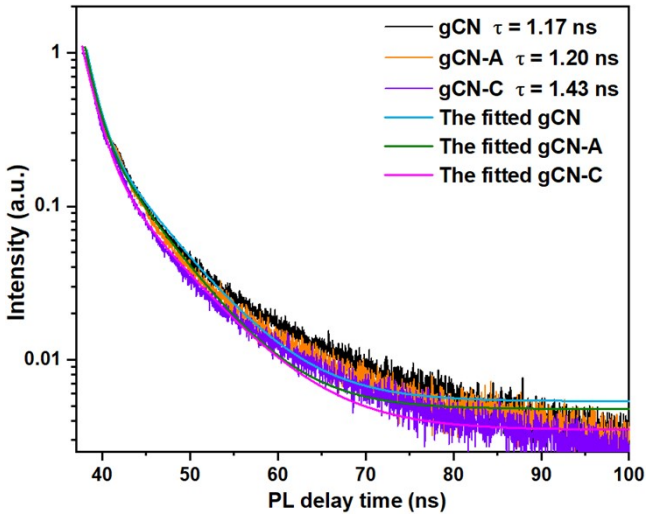

Fig. S10. Time-resolved PL spectra of gCN-A, gCN-C and intrinsic gCN (360 nm).

3.8. Dark adsorption observation

We added 30 min of dark adsorption observation and took samples at an interval of 10 min. As shown in Fig. S11, during the initial 10 min of dark adsorption, part of RhB will be adsorbed into the catalyst. After dark adsorption equilibrium is reached in 10 to 20 min, the corresponding C_t/C_0 values are defined. After that, the C_t/C_0 values remained almost constant for 20 to 30 min. Therefore, before the photocatalytic degradation reaction, the catalyst and degradation molecules were first subjected to dark adsorption for up to 30 min in order to fully achieve adsorption equilibrium.

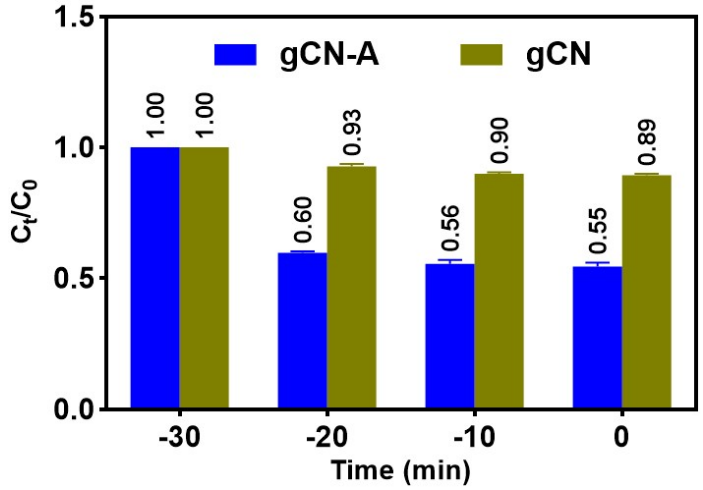

Fig. S11. Dark adsorption of RhB (20 mg/L) by gCN and gCN-A within 30 min.

3.9. Photocatalytic performance of gCN-A at different wavelengths

According to the existing photocatalytic instrument built-in Settings (including one reactor irradiated by 365 nm light, one reactor irradiated by 395 nm light, one reactor irradiated by 420 nm light, six reactors irradiated by 450 nm light and one reactor irradiated by 510 nm light), we studied the RhB degradation activity of gCN-A and gCN under 365 nm, 395 nm, 420 nm and 510 nm respectively. As shown in Fig. S12, gCN-A and gCN exhibited approximately poor photocatalytic degradation activity in the near ultraviolet region (365 nm and 395 nm). However, in the visible region, gCN-A shows many times better catalytic performance than gCN at 420 nm, 450 nm, or 510 nm, especially at 510 nm. Therefore, to avoid overly arbitrary conclusions, we conclude that gCN-A has the potential to perform better than substrate gCN under sunlight.

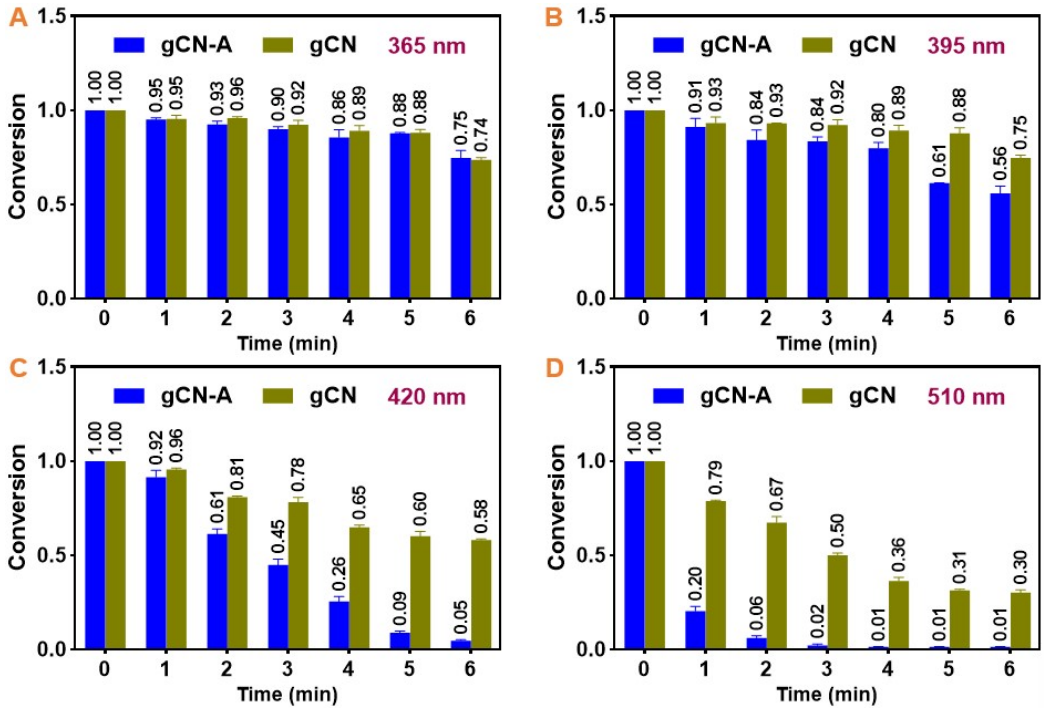

Fig. S12. Conversion of catalyst gCN and gCN-A to RhB under different wavelengths of light.

3.10. Degradation kinetic model

In order to reconfirm the kinetic model of gCN-A, the degradation of RhB by gCN-A under visible light was tested again. After 6 min of illumination, the degradation rate of RhB by gCN-A reached more than 95%. To better reflect the photocatalytic activity of gCN-A, only 0 to 6 min were used for kinetic simulation fitting, while other catalysts were fitted within 10 min. The degradation rate of RhB by gCN-A is 0.5319 min^{-1}, R^2 = 0.955 (Fig. 4). We chose the pseudo-first-order kinetic model based on the support of relevant literature and the observation of previous data.[3-5] We believe that this model can well describe the photocatalytic degradation behavior of materials, and the R^2 of gCN-A is close to 1, which indicates a good fit between the model and the experimental data. This result supports our belief that first-order kinetics model is appropriate when describing these data.

4. Material reusability

Reusability and stability serve as crucial benchmarks for the practical implementation of photocatalysts. We chose RhB as the subject of the reusability experiment because

RhB is more visually distinguishable in degradation and easy to detect in batches. The removal of RhB by gCN-A still exceeded 95% after five cycles (Fig. S13), highlighting the excellent photocatalytic performance of gCN-A. Concurrently, XRD, SEM, and FT-IR analysis (Fig. S14) revealed no significant alteration in gCN-A microscopic/chemical structure, affirming its remarkable built-in stability and economic viability.[6,7]

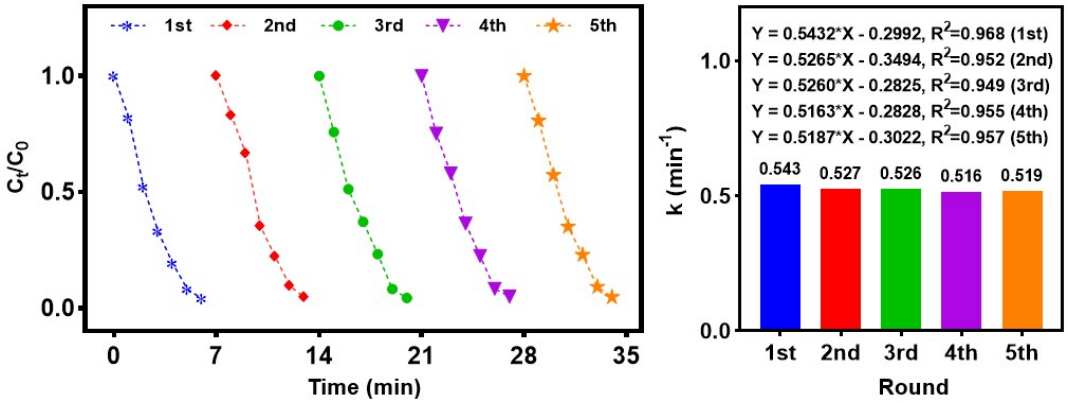

Fig. S13. Cycle measurement of RhB degradation and derived rate constants vs cycle round catalyzed by gCN-A.

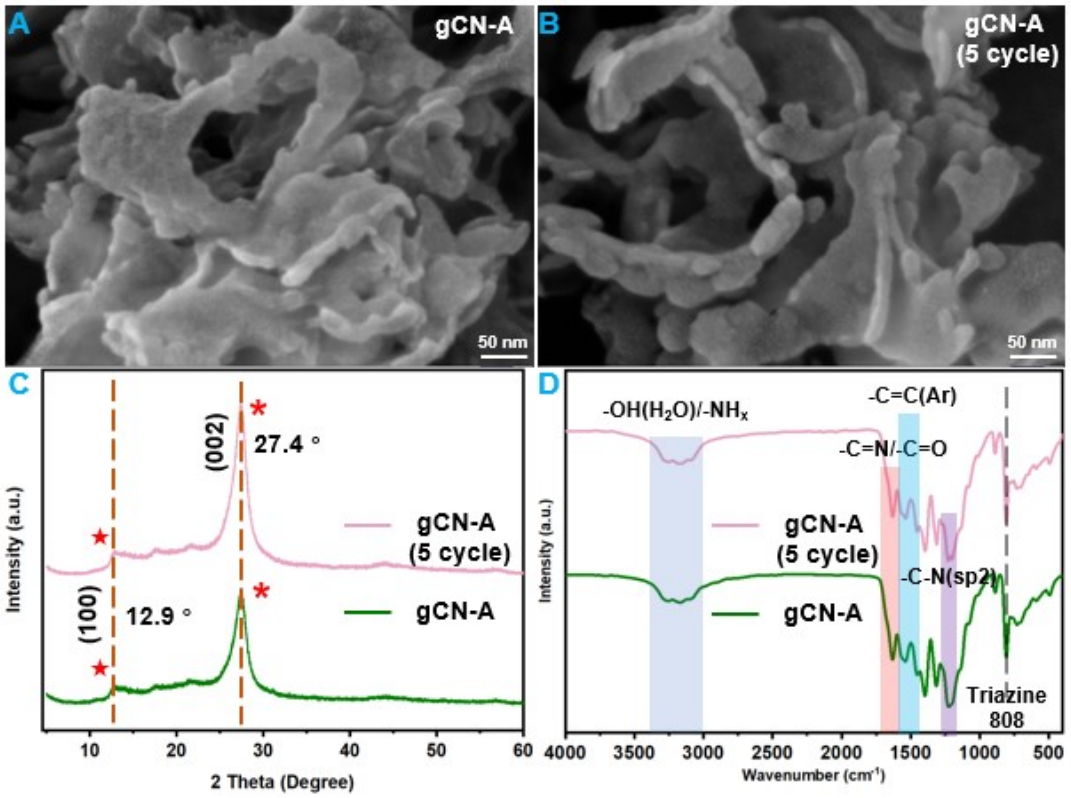

Fig. S14. The SEM imagine (A and B), XRD (C) and FT-IR (D) spectrum comparison between gCN-A and gCN-A (after five cycles).

5. High resolution of tetracycline degradation intermediates

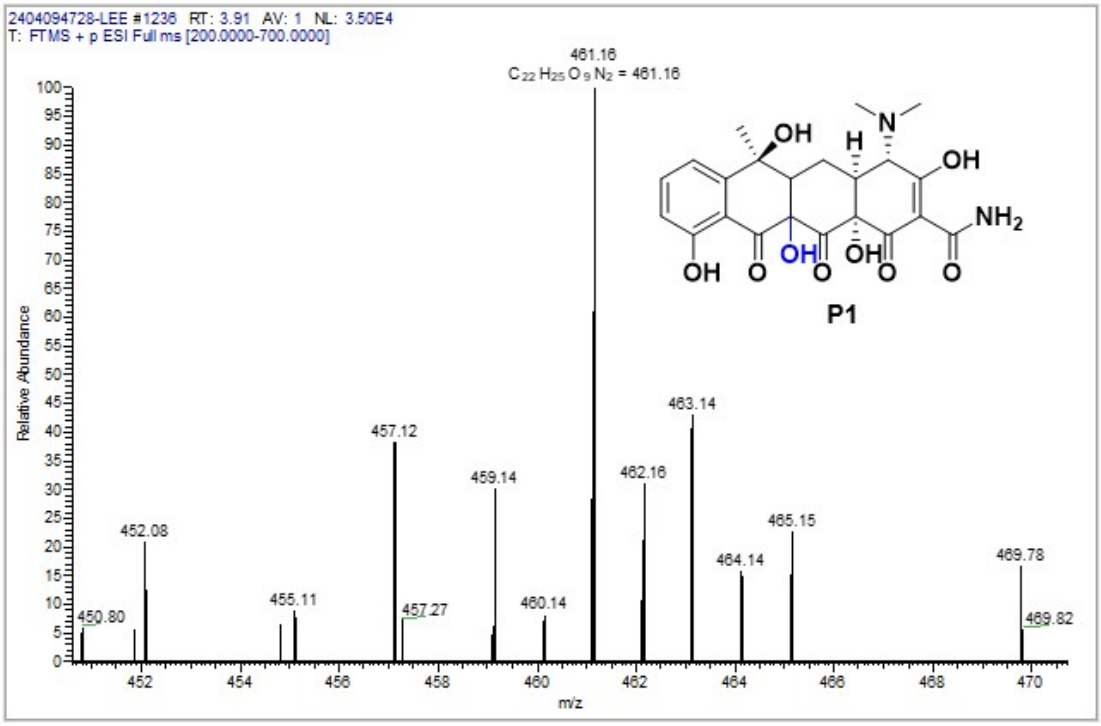

Fig. S15. Mass spectrometry analysis of intermediate P1.

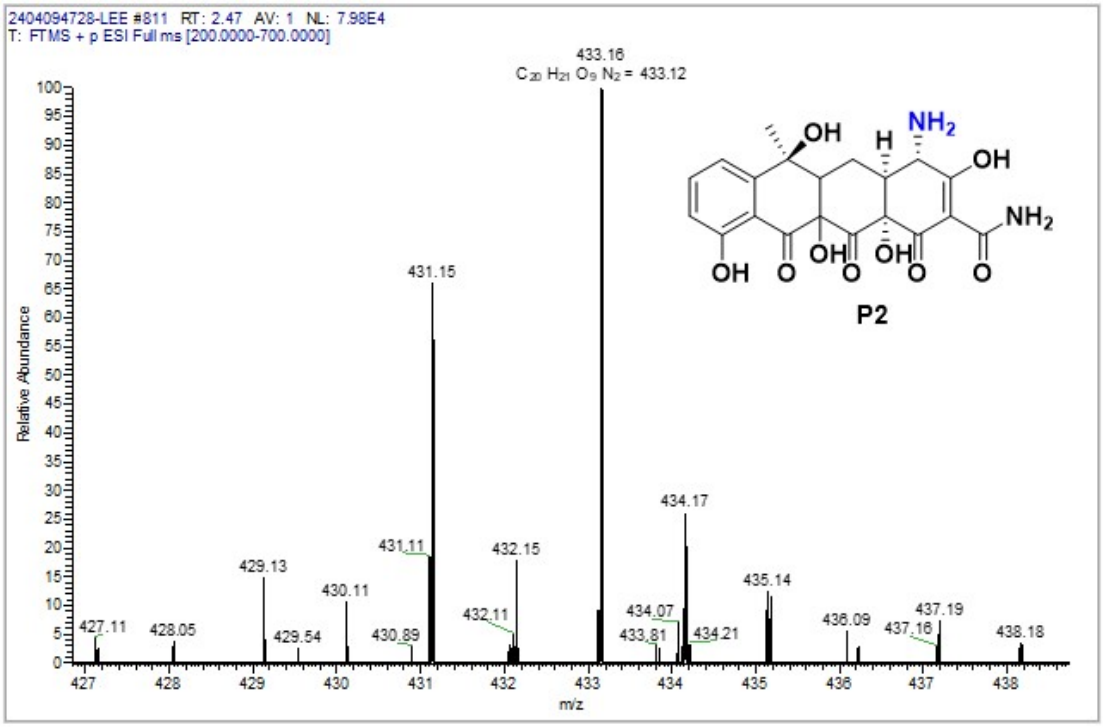

Fig. S16. Mass spectrometry analysis of intermediate P2.

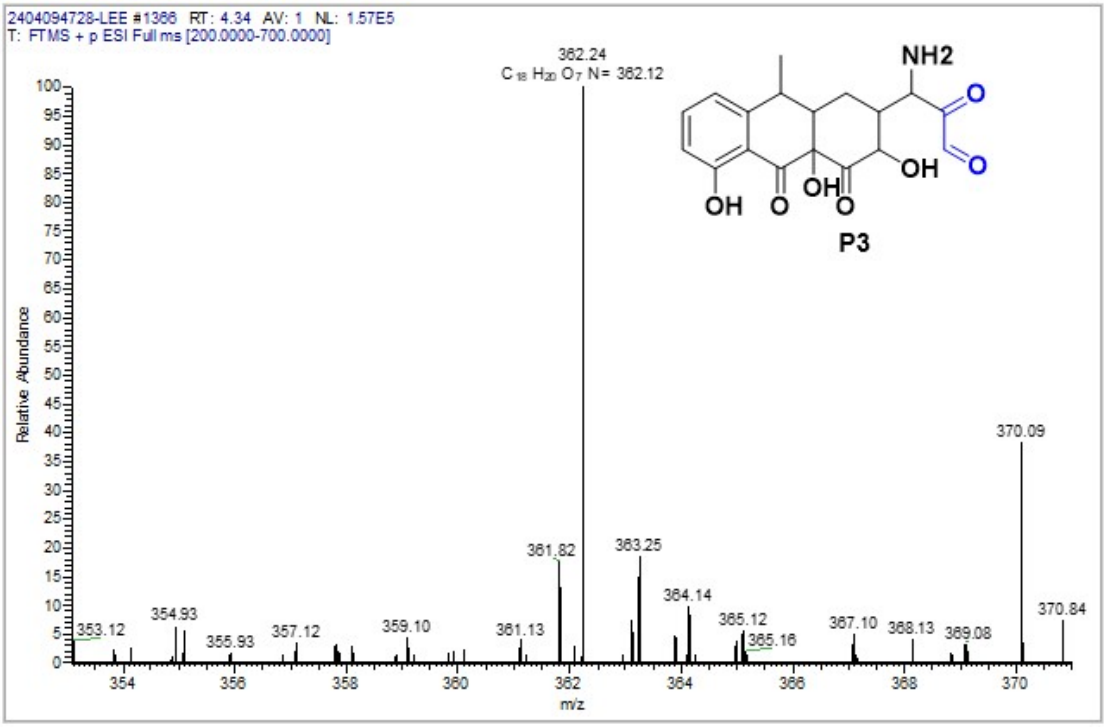

Fig. S17. Mass spectrometry analysis of intermediate P3

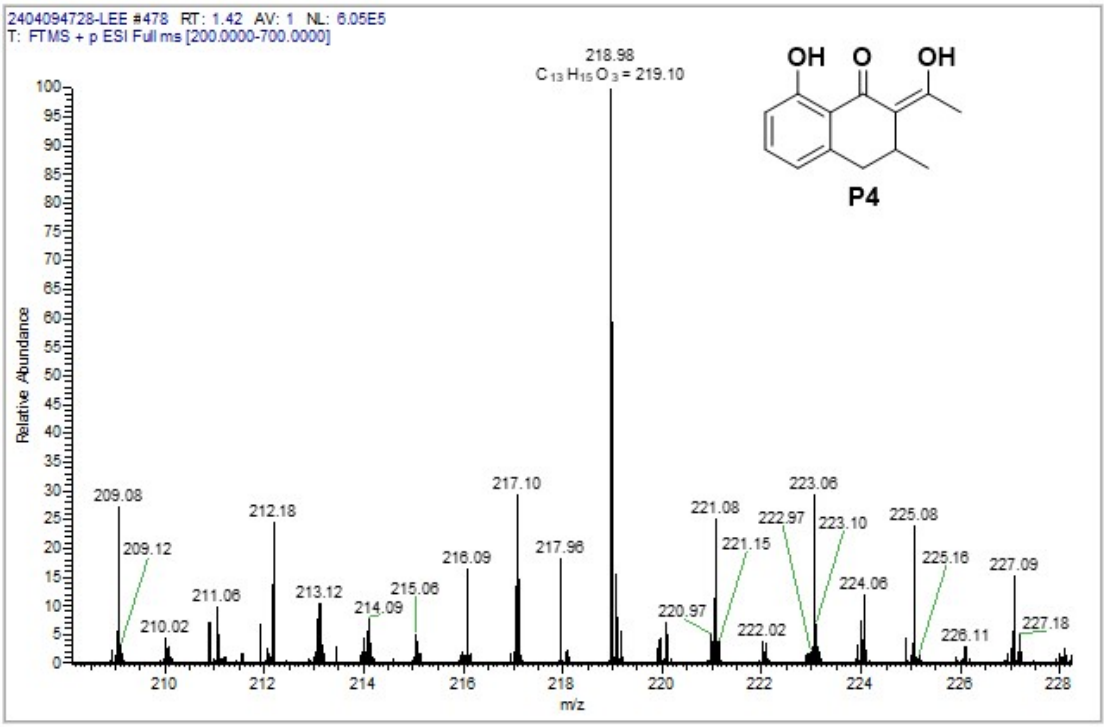

Fig. S18. Mass spectrometry analysis of intermediate P4.

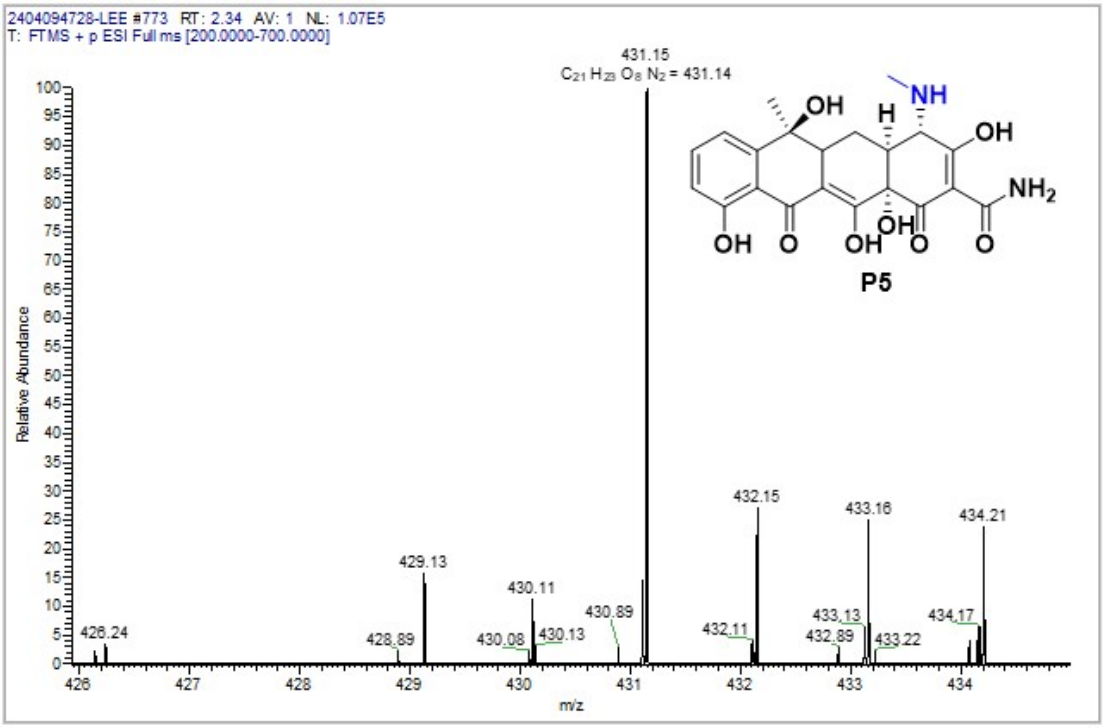

Fig. S19. Mass spectrometry analysis of intermediate P5.

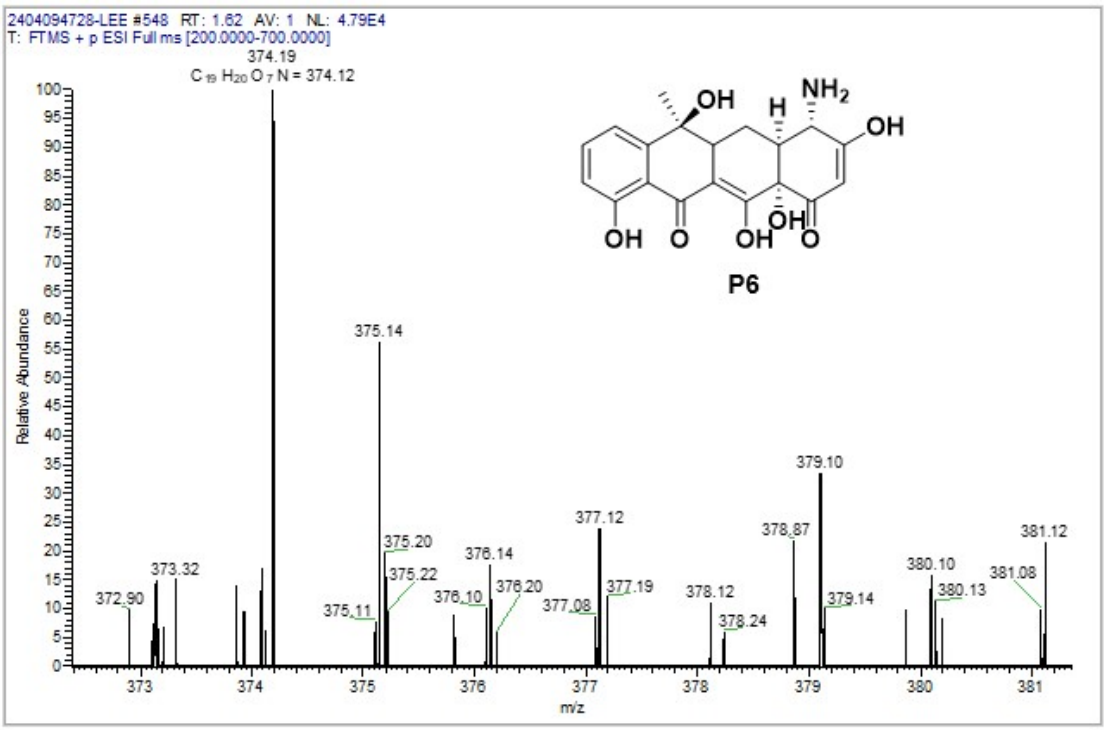

Fig. S20. Mass spectrometry analysis of intermediate P6.

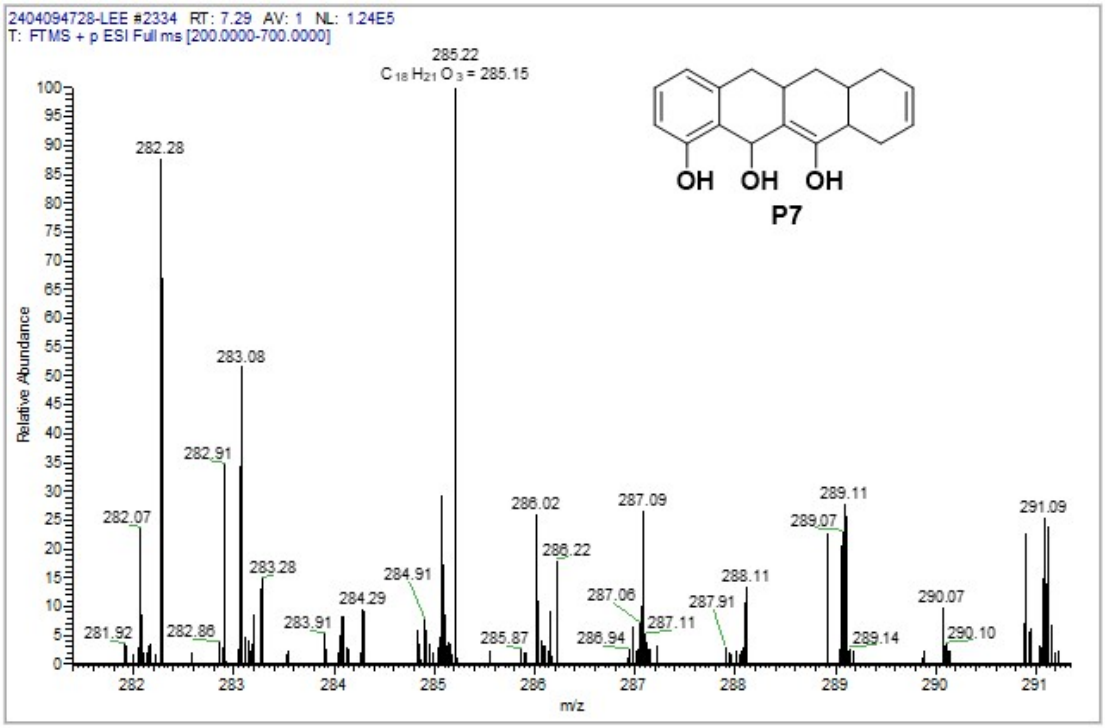

Fig. S21. Mass spectrometry analysis of intermediate P7.

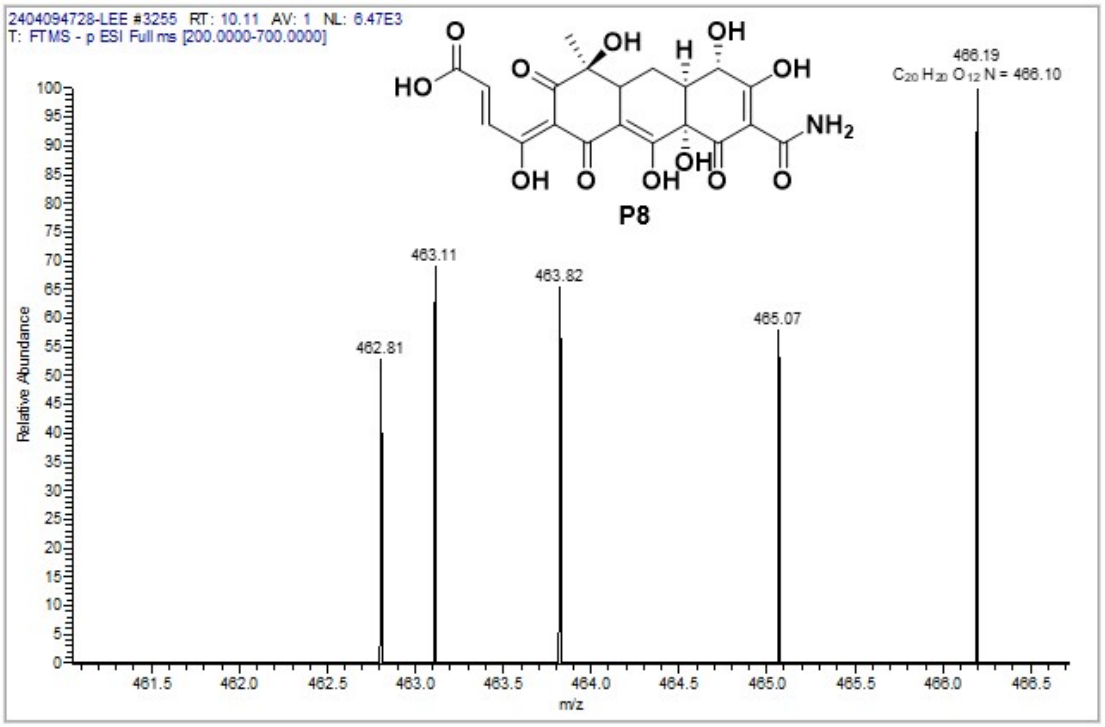

Fig. S22. Mass spectrometry analysis of intermediate P8.

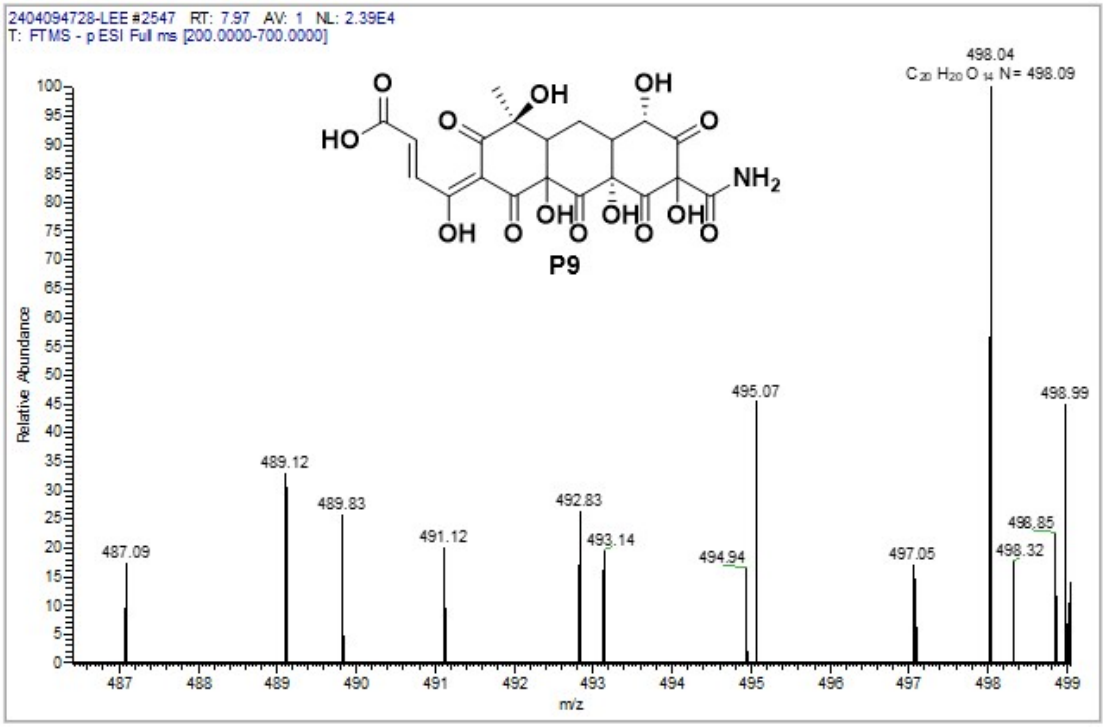

Fig. S23. Mass spectrometry analysis of intermediate P9.

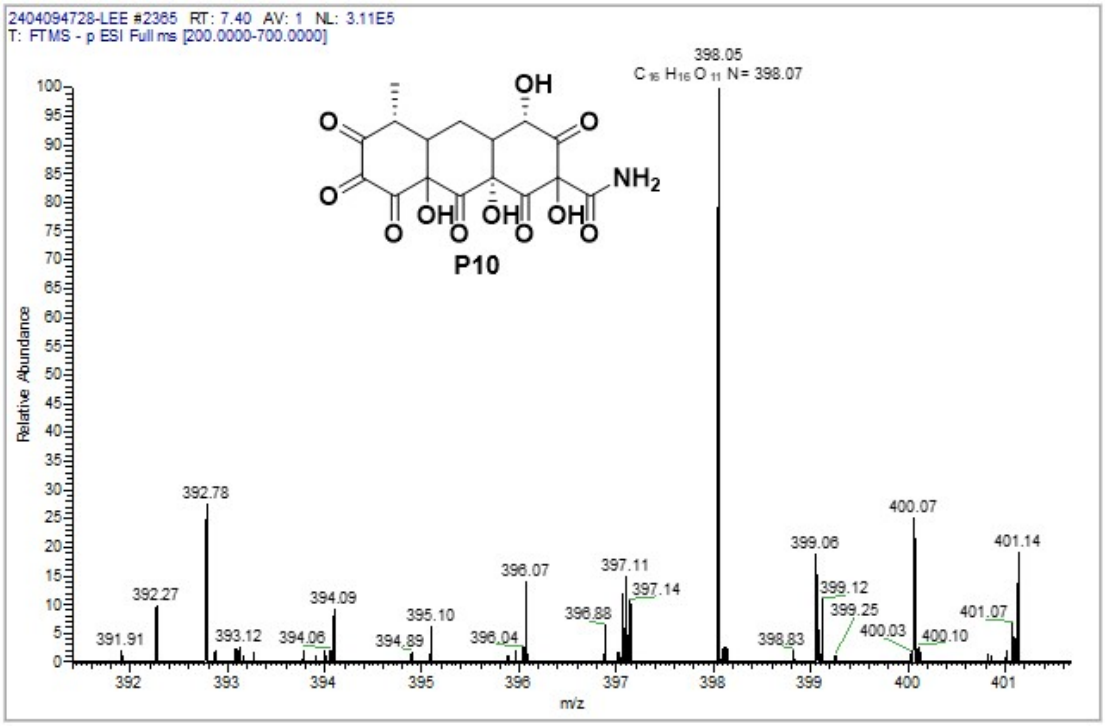

Fig. S24. Mass spectrometry analysis of intermediate P10.

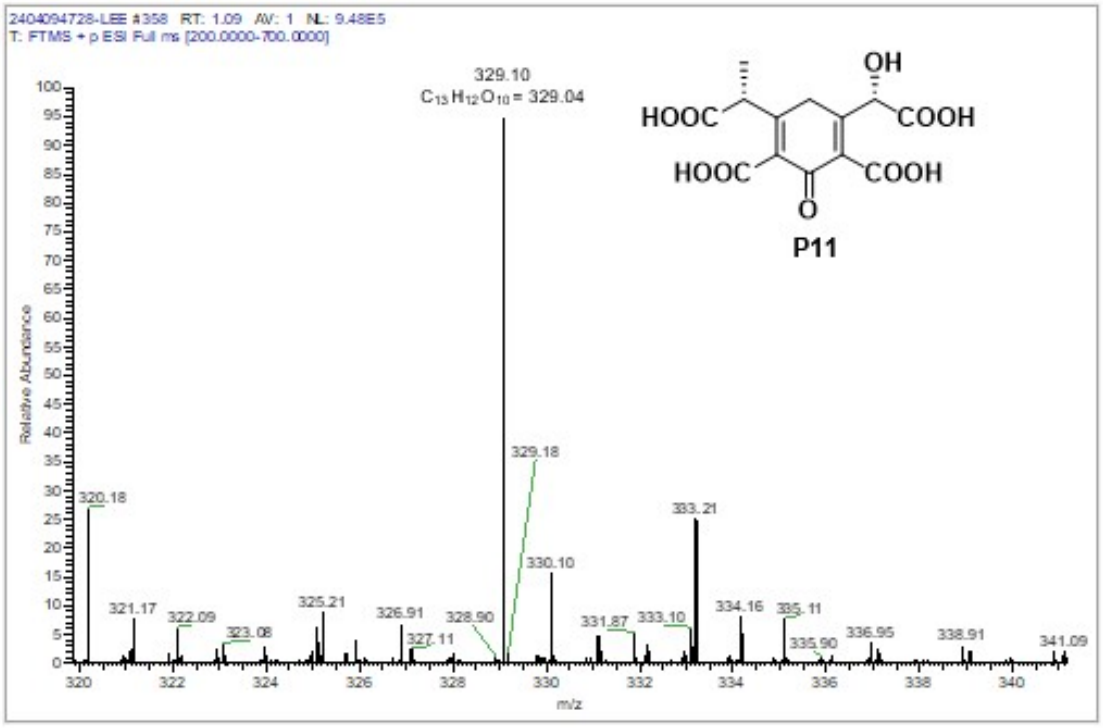

Fig. S25. Mass spectrometry analysis of intermediate P11.

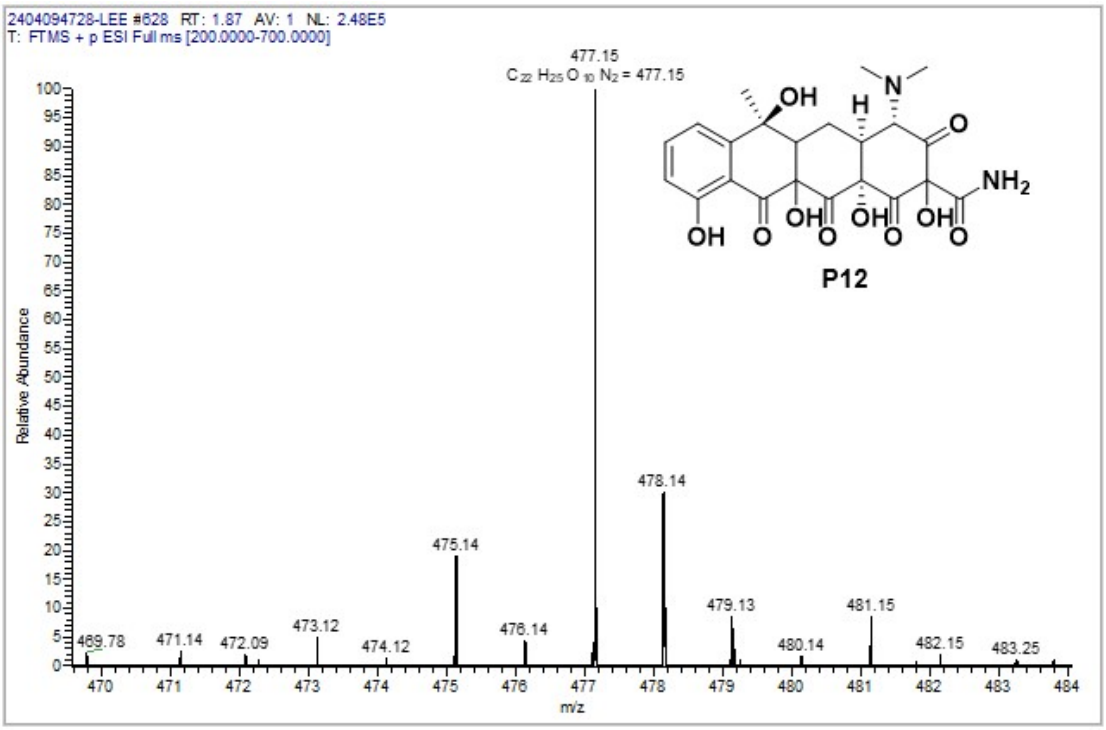

Fig. S26. Mass spectrometry analysis of intermediate P12.

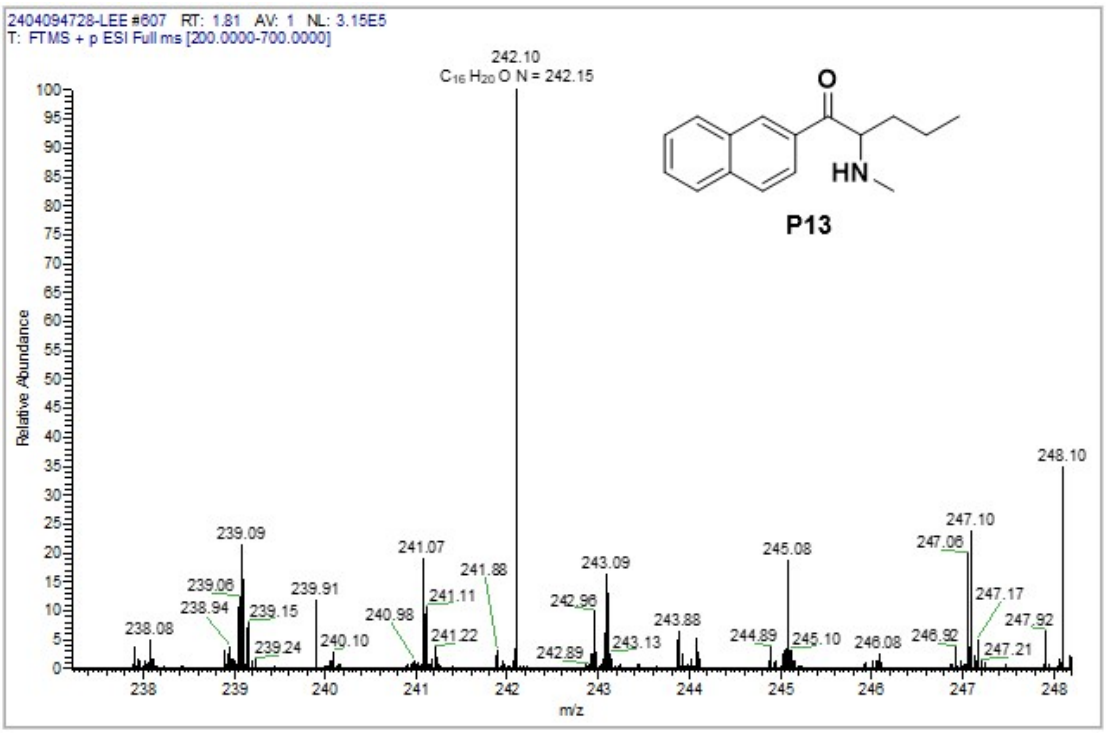

Fig. S27. Mass spectrometry analysis of intermediate P13.

6. Mineralization assay

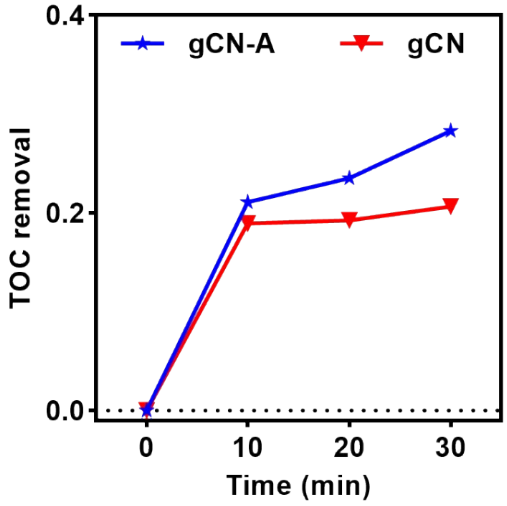

Fig. S28. The TOC removal (%) of TC in gCN and gCN-A.

7. Electron-hole calculation

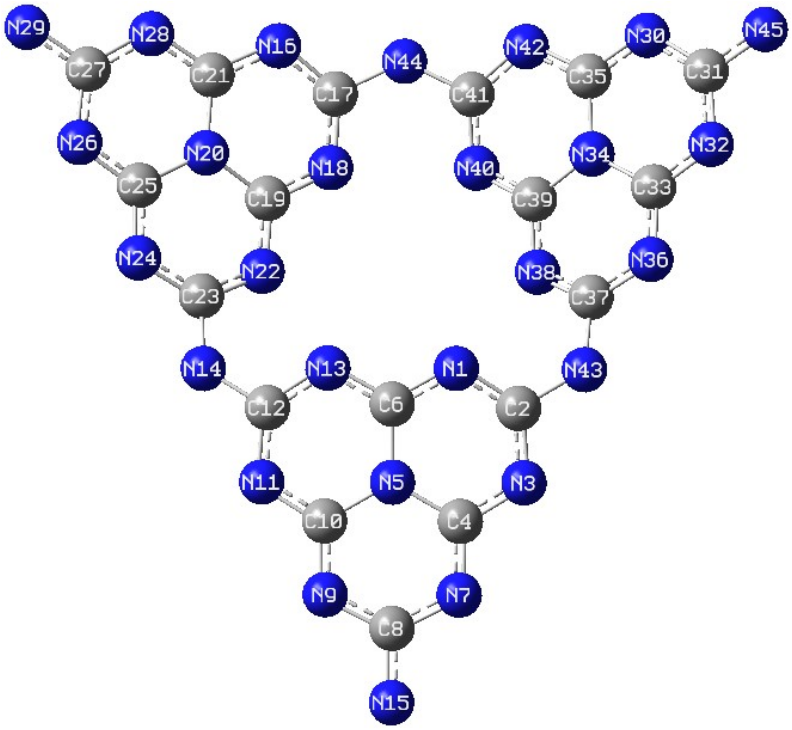

Fig. S29. Unit building structure and atomic number of gCN.

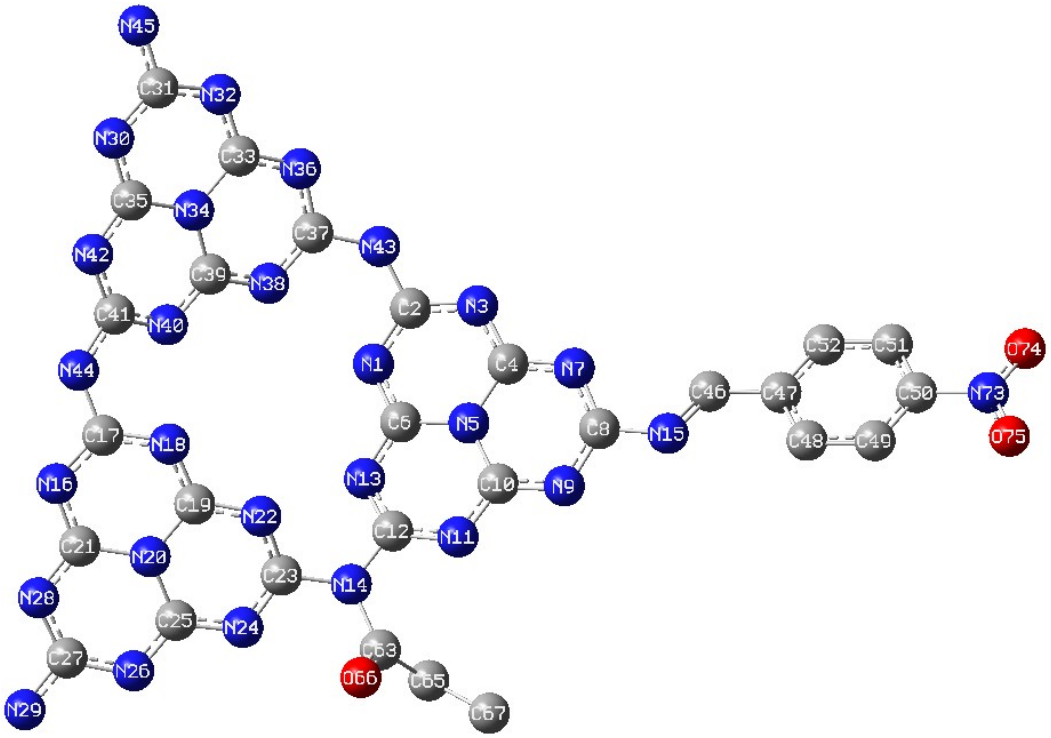

Fig. S30. Unit building structure and atomic number of gCN-A.

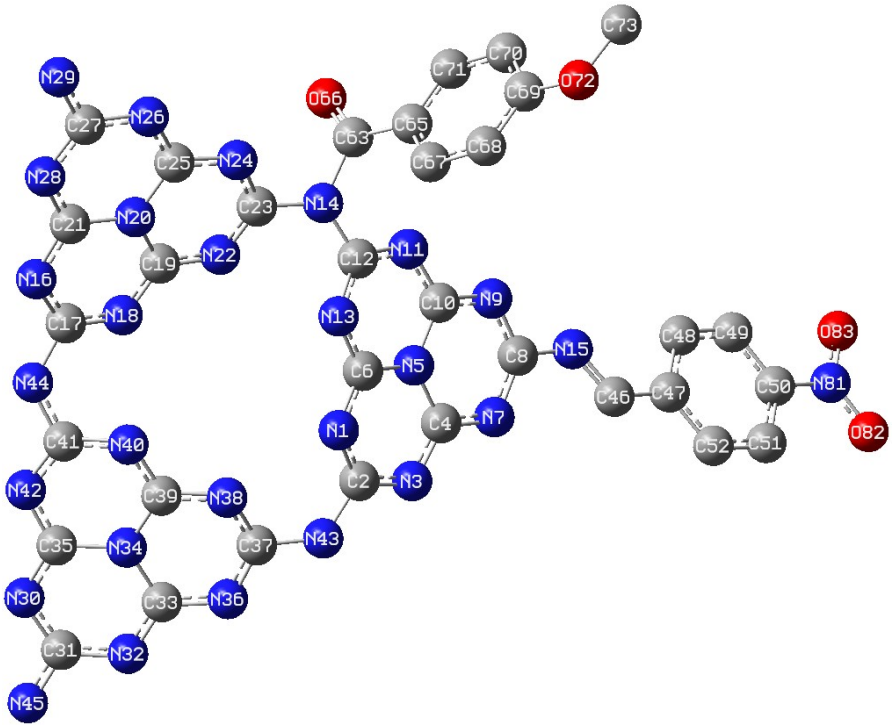

Fig. S31. Unit building structure and atomic number of gCN-B.

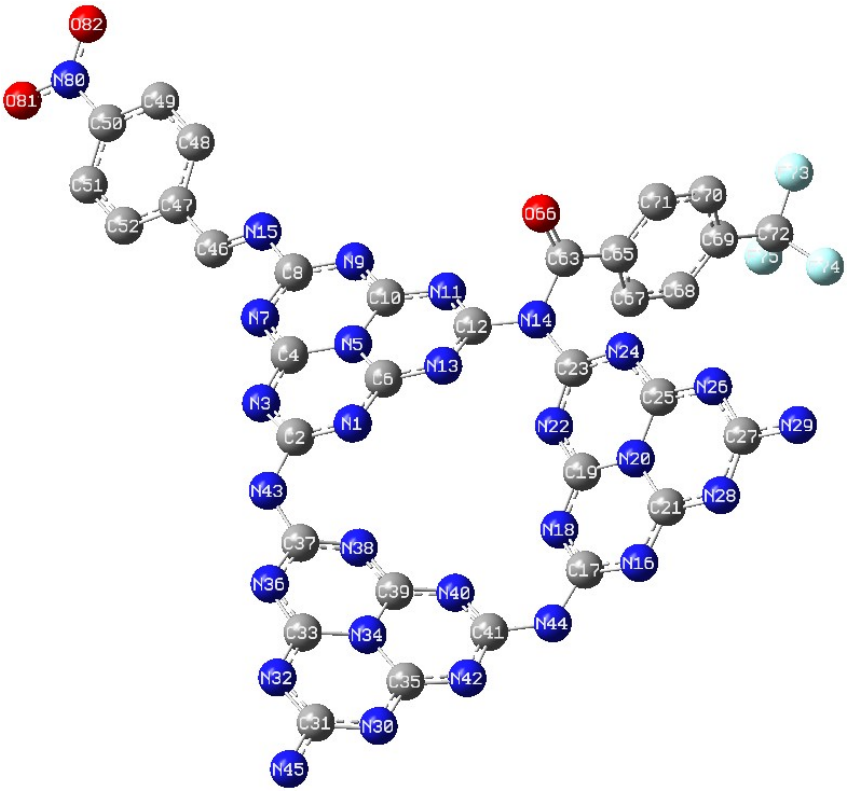

Fig. S32. Unit building structure and atomic number of gCN-C.

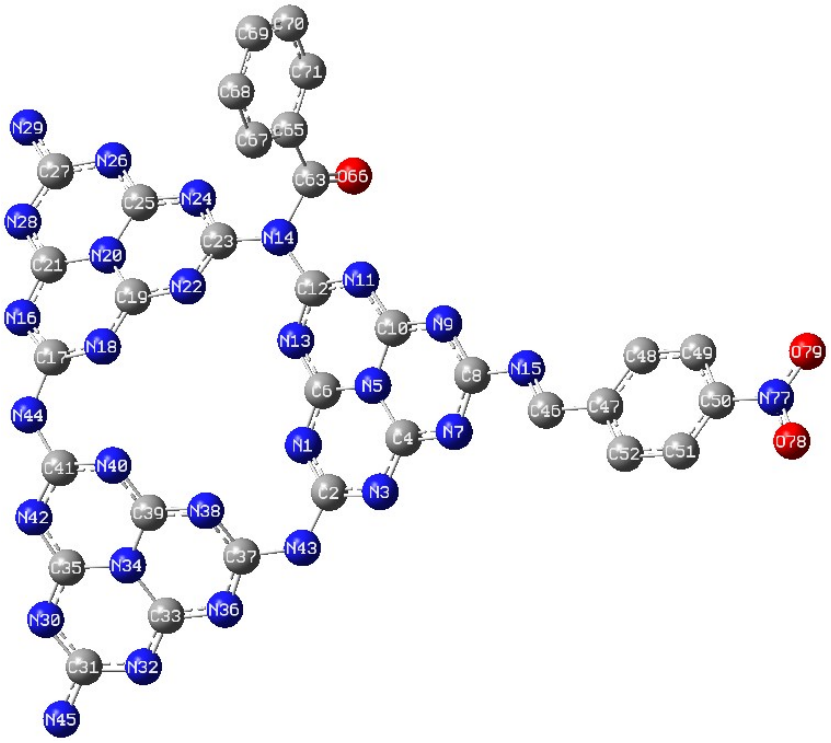

Fig. S33. Unit building structure and atomic number of gCN-D.

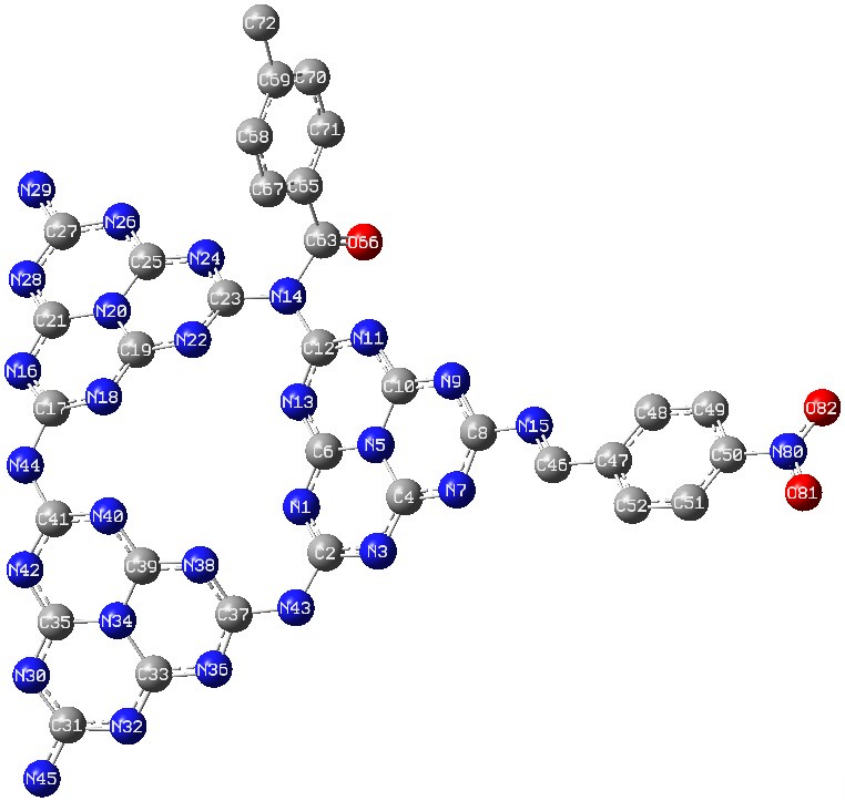

Fig. S34. Unit building structure and atomic number of gCN-E.

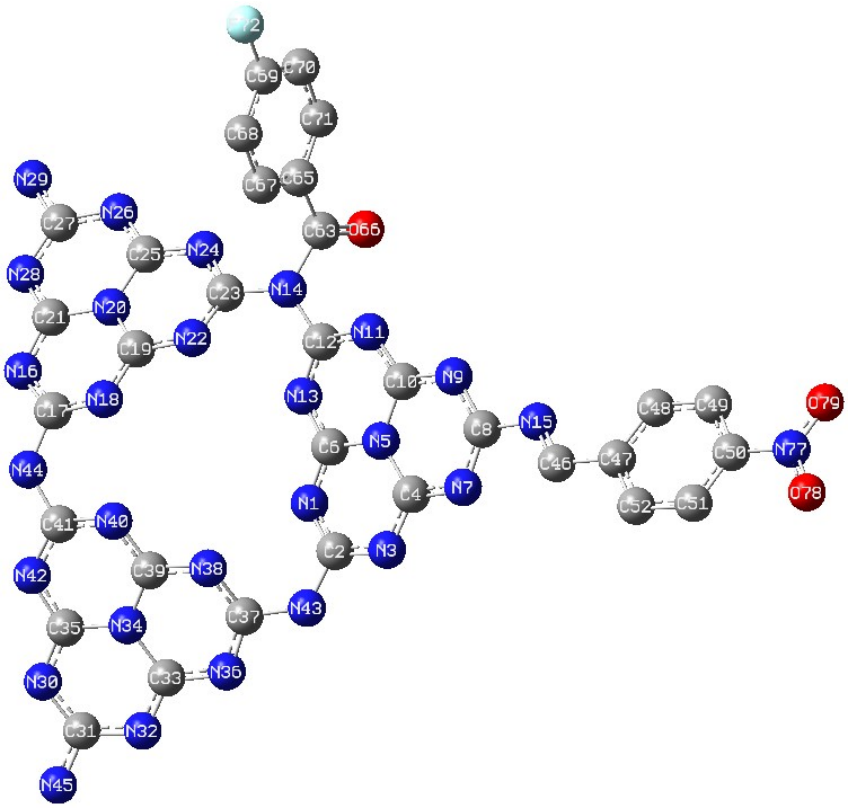

Fig. S35. Unit building structure and atomic number of gCN-F.

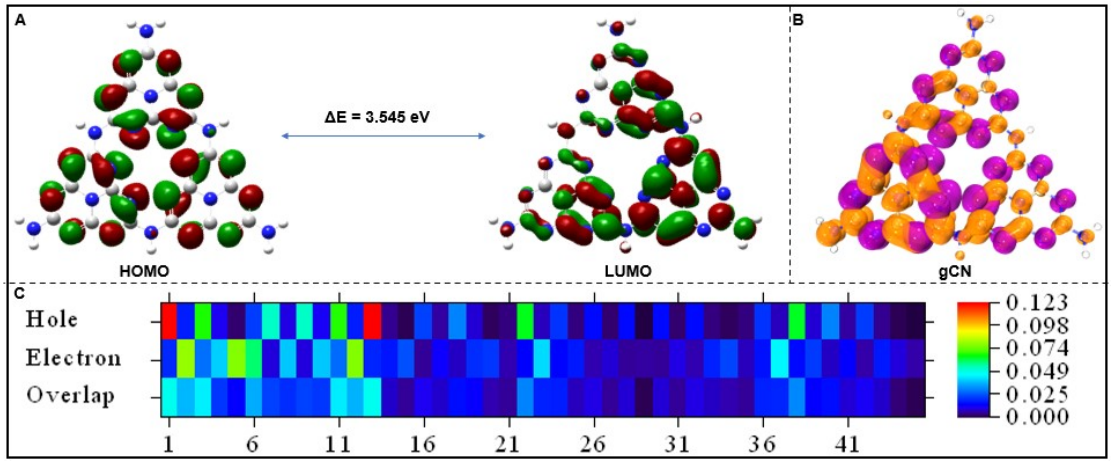

Fig. S36. The LUMO, HOMO and electron-hole distributions of gCN and the heat map (first excited state) display.

8. ROS observation

Fig. S37 demonstrates that no ROS was detected in the *Psa* cell system under visible light radiation (30 min) with 1% DMSO. In contrast, a weak ROS signal was observed in *Psa* containing gCN, while bacteria treated with gCN-A exhibited an enhanced ROS fluorescence signal, which was further supported by the gCN-A antibacterial evaluation and EPR detection.

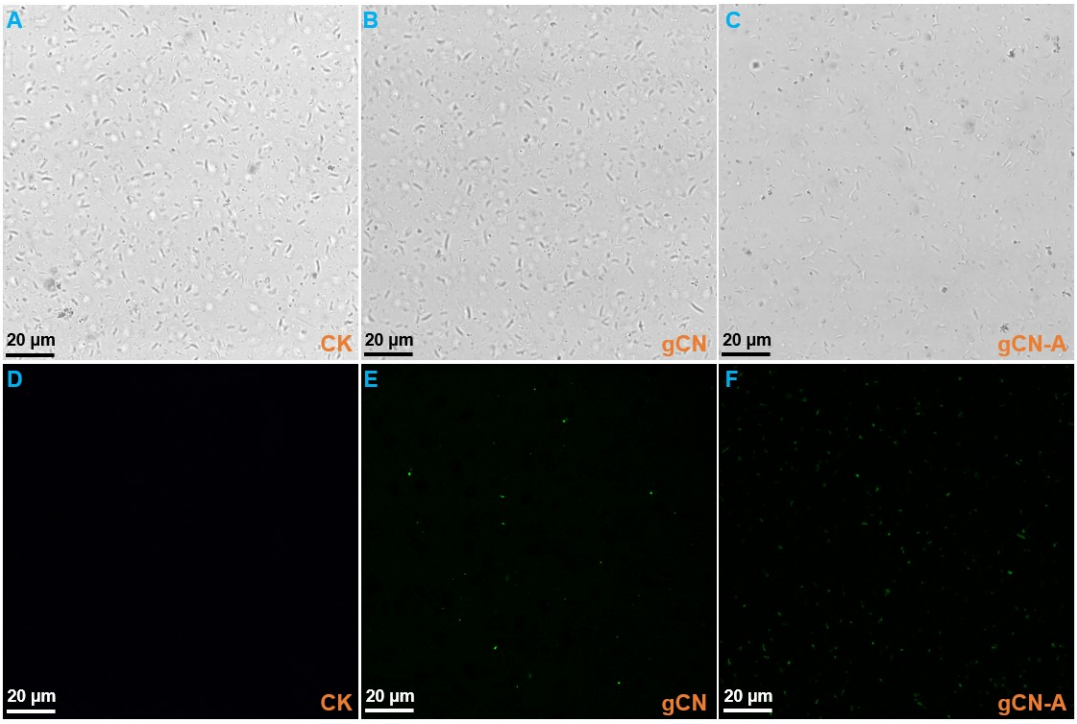

Fig. S37. Fluorescence image of the *Psa* cell dyed by CM-H_2DCFDA after treatment with 1% DMSO (A and D), gCN (B and E) or gCN-A (C and F) for 30 min, respectively. Scale bars = 20 μm.

9. Pesticide degradation plant toxicity test

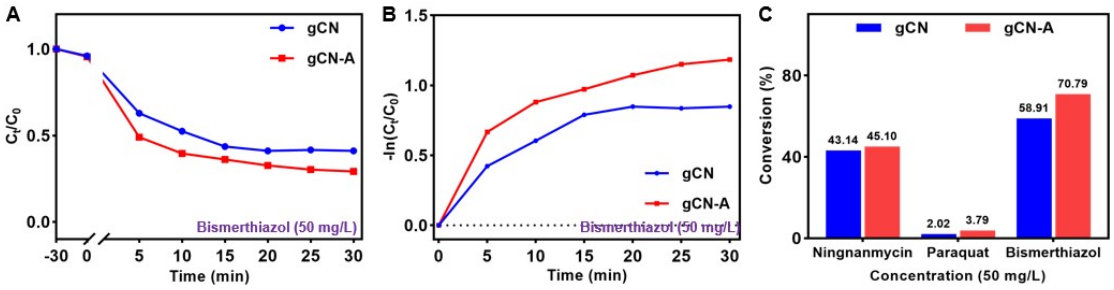

Fig. S38. Degradation curve and degradation rate fitting of Bismerthiazol by gCN-A under visible light irradiation. Conversion rate of gCN-A to Ningnanmycin, Paraquat, and Bismerthiazol at 50 mg/L.

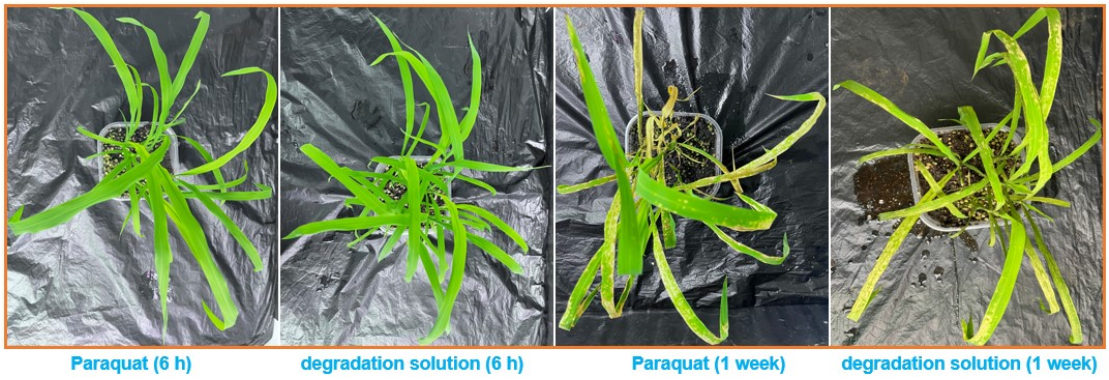

Fig. S39. Toxicity of Paraquat solution (50 mg/L) and its degradation products to rice seedlings.

Fig. S40. Toxicity of Paraquat solution (50 mg/L) and its degradation products to *Nicotiana glutinosa L*.

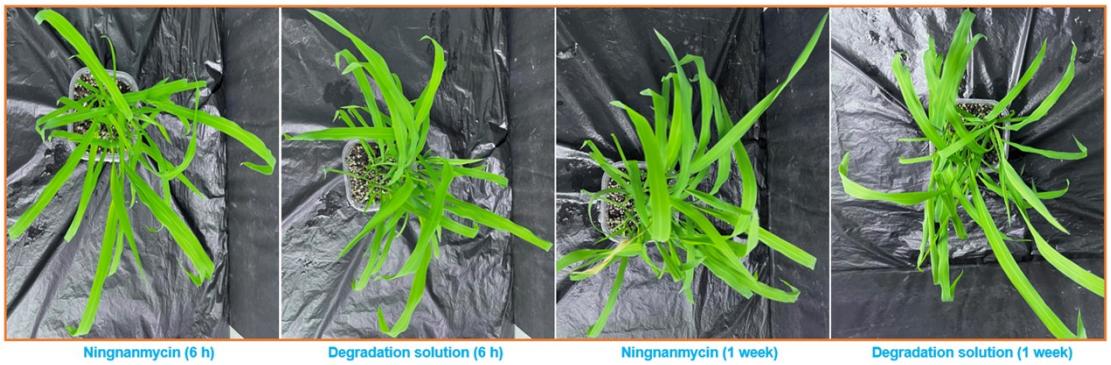

Fig. S41. Toxicity of Ningnanmycin solution (50 mg/L) and its degradation products to rice seedlings.

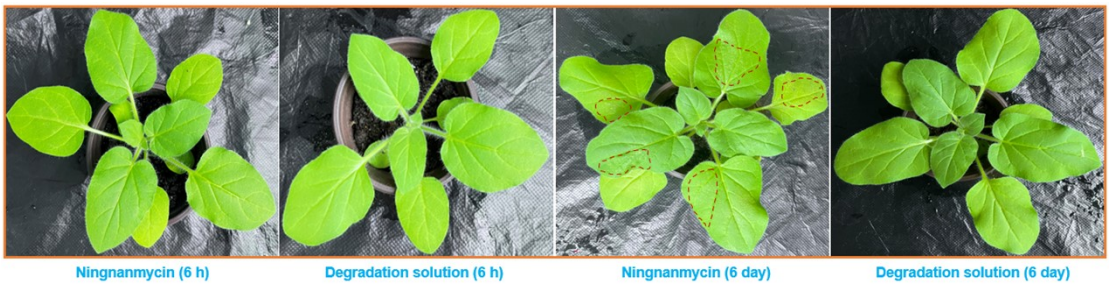

Fig. S42. Toxicity of Ningnanmycin solution (50 mg/L) and its degradation products to *Nicotiana glutinosa L*.

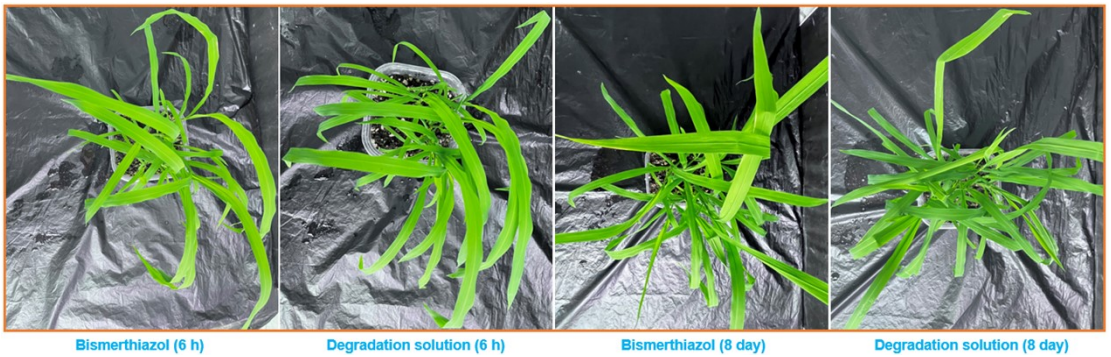

Fig. S43. Toxicity of Bismerthiazol solution (50 mg/L) and its degradation products to rice seedlings.

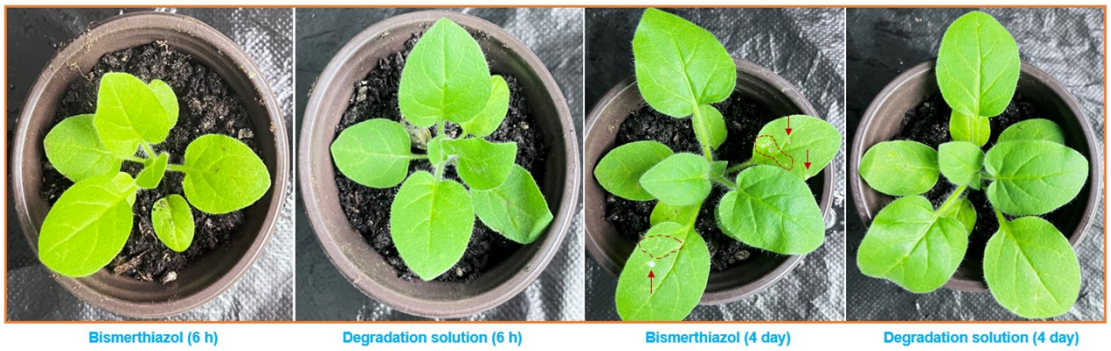

Fig. S44. Toxicity of Bismerthiazol solution (50 mg/L) and its degradation products to *Nicotiana glutinosa L*.

10. Relevant tables

Table S1. The BET surface area, average pore size, and pore volume measurement of gCN-based materials.

Sample	BET surface area (m^2/g)	Desorption average pore size (nm)	Adsorption average pore size (nm)	pore volume (cm^3/g)
gCN	44.645	12.804	13.257	0.124
gCN580	76.507	16.012	17.24	0.319
gCN-A	84.773	18.975	20.424	0.385
gCN-B	91.56	18.498	19.892	0.413
gCN-C	89.375	19.431	20.94	0.421

Table S2. DFT calculation of catalyst LUMO-HOMO energy.

Catalyst	LUMO (au)	LUMO (eV)	HOMO (au)	HOMO (eV)	ΔE
gCN	-0.097	-2.631	-0.227	-6.176	3.545
gCN-A	-0.135	-3.683	-0.238	-6.475	2.792
gCN-B	-0.133	-3.607	-0.234	-6.375	2.769
gCN-C	-0.136	-3.692	-0.241	-6.556	2.864
gCN-D	-0.133	-3.608	-0.237	-6.434	2.827
gCN-E	-0.132	-3.592	-0.236	-6.410	2.818
gCN-F	-0.134	-3.647	-0.239	-6.490	2.843

1 au = 1*27.21138602 eV

Table S3. Contribution of each non-hydrogen atom to hole and electron in gCN.

Atom	Hole (%)	Electron (%)	Overlap	Atom	Hole (%)	Electron (%)	Overlap
1	12.233	1.919	4.845	24	2.064	1.497	1.758
2	1.754	8.005	3.747	25	0.35	1.696	0.77
3	6.816	2.853	4.409	26	1.509	0.631	0.976
4	1.114	4.032	2.119	27	0.285	0.905	0.507
5	0.246	7.836	1.387	28	1.531	0.505	0.879
6	2.181	6.003	3.618	29	0.034	0.536	0.136

7	5.289	0.951	2.243	30	1.506	0.511	0.877
8	0.981	3.931	1.963	31	0.282	0.983	0.526
9	5.292	0.946	2.237	32	1.502	0.645	0.984
10	1.116	3.961	2.103	33	0.348	1.823	0.797
11	6.833	2.806	4.379	34	0.19	2.312	0.663
12	1.763	7.844	3.719	35	0.377	0.727	0.524
13	12.306	1.873	4.802	36	2.061	1.619	1.827
14	0.447	1.668	0.864	37	0.764	4.511	1.856
15	0.115	2.462	0.532	38	6.47	1.508	3.123
16	2.24	0.531	1.091	39	0.903	2.143	1.391
17	0.571	1.28	0.855	40	3.07	0.793	1.56
18	3.099	0.782	1.557	41	0.565	1.405	0.891
19	0.913	1.949	1.334	42	2.2	0.59	1.14
20	0.192	2.094	0.635	43	0.438	1.697	0.862
21	0.383	0.677	0.51	44	0.108	0.937	0.318
22	6.537	1.453	3.082	45	0.034	0.59	0.142
23	0.771	4.2	1.799	□	□	□	□

Table S4. Contribution of each non-hydrogen atom to hole and electron in gCN-A.

Atom	Hole (%)	Electron (%)	Overlap	Atom	Hole (%)	Electron (%)	Overlap
1	9.532	0.793	2.749	31	0.359	0.054	0.14
2	1.781	1.756	1.768	32	1.796	0.083	0.386
3	7.832	0.651	2.258	33	0.472	0.173	0.286
4	1.509	2.64	1.996	34	0.108	0.155	0.129
5	0.198	4.412	0.936	35	0.374	0.039	0.121
6	1.897	1.416	1.639	36	2.577	0.197	0.712
7	6.741	3.011	4.506	37	0.861	0.454	0.625
8	1.394	7.45	3.223	38	5.521	0.23	1.126
9	6.454	2.929	4.348	39	0.997	0.148	0.384
10	1.275	3.646	2.156	40	4.096	0.079	0.57
11	6.175	0.971	2.448	41	0.649	0.056	0.191
12	1.583	2.386	1.944	42	1.946	0.047	0.303
13	9.319	1.148	3.271	43	0.166	0.496	0.287
14	0.2	0.697	0.374	44	0.204	0.034	0.083
15	0.116	7.729	0.947	45	0.04	0.03	0.035
16	2.156	0.023	0.224	46	0.048	12.123	0.762
17	0.683	0.034	0.153	47	0.009	5.085	0.216
18	4.285	0.052	0.471	48	0.004	3.757	0.12
19	0.962	0.083	0.283	49	0.002	2.498	0.063
20	0.092	0.1	0.096	50	0.004	5.366	0.142
21	0.407	0.03	0.111	51	0.002	2.865	0.076
22	5.07	0.203	1.015	52	0.002	3.671	0.081
23	0.821	0.419	0.586	63	0.071	0.19	0.116
24	2.632	0.175	0.678	65	0.055	0.052	0.053

25	0.492	0.139	0.262	66	0.124	0.117	0.121
26	1.946	0.077	0.387	67	0.013	0.014	0.013
27	0.393	0.047	0.135	73	0	5.346	0.047
28	1.751	0.042	0.27	74	0.001	5.598	0.06
29	0.037	0.026	0.031	75	0.001	5.687	0.053
30	1.562	0.049	0.276	□	□	□	□

Table S5. Contribution of each non-hydrogen atom to hole and electron in gCN-B.

Atom	Hole (%)	Electron (%)	Overlap	Atom	Hole (%)	Electron (%)	Overlap
1	10.356	0.765	2.815	34	0.099	0.142	0.118
2	1.958	1.703	1.826	35	0.284	0.039	0.105
3	8.5	0.625	2.306	36	2.073	0.183	0.617
4	1.647	2.556	2.052	37	0.719	0.419	0.549
5	0.212	4.233	0.946	38	4.713	0.215	1.008
6	2.08	1.357	1.68	39	0.83	0.137	0.337
7	7.465	2.839	4.604	40	3.256	0.077	0.5
8	1.567	7.016	3.316	41	0.513	0.055	0.168
9	7.319	2.832	4.552	42	1.437	0.038	0.234
10	1.459	3.421	2.234	43	0.158	0.485	0.277
11	7.096	0.903	2.532	44	0.203	0.048	0.099
12	1.744	2.286	1.997	45	0.035	0.028	0.031
13	10.293	1.11	3.379	46	0.056	11.585	0.804
14	0.197	0.627	0.352	47	0.011	5.217	0.234
15	0.13	7.699	1	48	0.004	3.707	0.119
16	1.821	0.037	0.26	49	0.002	2.605	0.066
17	0.599	0.057	0.185	50	0.003	5.411	0.133
18	3.692	0.064	0.486	51	0.002	3.031	0.076
19	0.884	0.127	0.335	52	0.002	3.578	0.086
20	0.091	0.153	0.118	63	0.098	0.135	0.115
21	0.343	0.045	0.124	65	0.191	0.05	0.098
22	4.841	0.235	1.067	66	0.213	0.046	0.099
23	0.748	0.535	0.632	67	0.065	0.031	0.045
24	2.225	0.221	0.701	68	0.066	0.011	0.027
25	0.418	0.189	0.281	69	0.111	0.019	0.046
26	1.651	0.094	0.394	70	0.082	0.024	0.044
27	0.331	0.068	0.15	71	0.057	0.031	0.042
28	1.451	0.053	0.277	72	0.129	0.006	0.028
29	0.035	0.038	0.037	73	0.012	0.001	0.003
30	1.197	0.045	0.231	81	0	5.922	0.046
31	0.277	0.052	0.12	82	0.001	6.124	0.058
32	1.375	0.074	0.318	83	0	6.223	0.054
33	0.38	0.153	0.241	□	□	□	□

Table S6. Contribution of each non-hydrogen atom to hole and electron in gCN-C.

Atom	Hole (%)	Electron (%)	Overlap	Atom	Hole (%)	Electron (%)	Overlap
1	12.675	1.039	3.629	35	0.295	0.052	0.124
2	2.17	2.951	2.531	36	1.82	0.345	0.792
3	8.908	0.827	2.713	37	0.663	0.769	0.714
4	1.751	3.262	2.39	38	5.093	0.308	1.252
5	0.231	5.568	1.135	39	0.788	0.223	0.42
6	2.472	2.202	2.333	40	2.103	0.103	0.466
7	8.412	2.788	4.843	41	0.419	0.066	0.167
8	1.828	7.468	3.694	42	1.53	0.072	0.331
9	8.84	2.849	5.018	43	0.198	0.752	0.385
10	1.885	3.825	2.685	44	0.044	0.037	0.04
11	9.697	0.91	2.971	45	0.037	0.032	0.034
12	2.232	3.307	2.717	46	0.093	11.012	1.015
13	11.768	1.352	3.989	47	0.025	4.438	0.33
14	0.16	0.71	0.337	48	0.009	3.307	0.169
15	0.243	7.068	1.311	49	0.004	2.193	0.092
16	1.094	0.019	0.146	50	0.005	4.713	0.152
17	0.287	0.026	0.087	51	0.003	2.453	0.084
18	1.406	0.053	0.273	52	0.005	3.301	0.123
19	0.448	0.096	0.207	63	0.071	0.318	0.15
20	0.079	0.12	0.097	65	0.02	0.046	0.03
21	0.211	0.032	0.083	66	0.118	0.334	0.198
22	2.801	0.255	0.845	67	0.018	0.043	0.027
23	0.403	0.533	0.463	68	0.006	0.012	0.009
24	1.076	0.198	0.462	69	0.008	0.027	0.015
25	0.217	0.192	0.204	70	0.006	0.013	0.008
26	0.916	0.108	0.315	71	0.009	0.025	0.015
27	0.183	0.059	0.104	72	0.001	0.005	0.002
28	0.799	0.064	0.227	73	0	0.001	0.001
29	0.021	0.03	0.025	74	0.001	0.003	0.001
30	1.114	0.071	0.281	75	0	0.001	0.001
31	0.264	0.062	0.128	80	0.001	4.594	0.05
32	1.355	0.132	0.422	81	0.001	4.833	0.063
33	0.344	0.241	0.288	82	0.001	4.902	0.069
34	0.159	0.209	0.182	□	□	□	□

Table S7. Contribution of each non-hydrogen atom to hole and electron in gCN-D.

Atom	Hole (%)	Electron (%)	Overlap	Atom	Hole (%)	Electron (%)	Overlap
1	12.581	0.977	3.505	33	0.311	0.246	0.277
2	2.184	2.567	2.368	34	0.147	0.189	0.166
3	8.944	0.75	2.59	35	0.287	0.043	0.112
4	1.752	3.065	2.317	36	1.615	0.268	0.658

5	0.223	5.122	1.07	37	0.608	0.661	0.634
6	2.473	1.873	2.153	38	4.708	0.294	1.177
7	8.372	2.741	4.79	39	0.732	0.158	0.34
8	1.819	7.332	3.652	40	1.979	0.068	0.368
9	8.722	2.946	5.069	41	0.398	0.046	0.136
10	1.839	3.649	2.591	42	1.475	0.042	0.25
11	9.378	0.856	2.833	43	0.199	0.654	0.361
12	2.195	2.871	2.51	44	0.042	0.032	0.037
13	11.891	1.226	3.818	45	0.029	0.041	0.034
14	0.176	0.671	0.344	46	0.094	11.124	1.021
15	0.231	7.235	1.292	47	0.024	4.734	0.334
16	1.256	0.037	0.215	48	0.008	3.341	0.165
17	0.337	0.035	0.109	49	0.003	2.418	0.085
18	1.663	0.076	0.356	50	0.005	4.955	0.151
19	0.526	0.129	0.261	51	0.002	2.615	0.079
20	0.092	0.125	0.107	52	0.004	3.471	0.117
21	0.239	0.04	0.098	63	0.07	0.187	0.114
22	3.258	0.242	0.888	65	0.036	0.019	0.026
23	0.46	0.561	0.508	66	0.112	0.182	0.143
24	1.244	0.237	0.543	67	0.027	0.022	0.024
25	0.249	0.182	0.213	68	0.012	0.007	0.009
26	1.035	0.116	0.346	69	0.024	0.008	0.014
27	0.206	0.045	0.096	70	0.013	0.003	0.007
28	0.895	0.065	0.24	71	0.016	0.007	0.011
29	0.023	0.021	0.022	77	0.001	5.169	0.052
30	1.093	0.071	0.279	78	0.001	5.397	0.066
31	0.251	0.076	0.138	79	0.001	5.459	0.068
32	1.252	0.122	0.391	□	□	□	□

Table S8. Contribution of each non-hydrogen atom to hole and electron in gCN-E.

Atom	Hole (%)	Electron (%)	Overlap	Atom	Hole (%)	Electron (%)	Overlap
1	12.651	0.966	3.495	33	0.305	0.238	0.269
2	2.192	2.475	2.329	34	0.152	0.182	0.166
3	8.853	0.735	2.552	35	0.279	0.042	0.108
4	1.736	3.023	2.291	36	1.593	0.26	0.644
5	0.224	4.999	1.058	37	0.612	0.64	0.626
6	2.48	1.789	2.106	38	4.764	0.284	1.162
7	8.284	2.723	4.749	39	0.737	0.153	0.336
8	1.805	7.286	3.626	40	1.95	0.066	0.359
9	8.667	2.972	5.076	41	0.393	0.045	0.132
10	1.829	3.58	2.559	42	1.443	0.041	0.242
11	9.307	0.839	2.795	43	0.212	0.629	0.365
12	2.185	2.747	2.45	44	0.042	0.032	0.037
13	11.877	1.187	3.755	45	0.028	0.039	0.033

14	0.181	0.655	0.344	46	0.093	11.163	1.017
15	0.229	7.294	1.293	47	0.024	4.813	0.336
16	1.281	0.038	0.22	48	0.009	3.354	0.17
17	0.344	0.035	0.11	49	0.004	2.477	0.093
18	1.689	0.077	0.36	50	0.005	5.018	0.159
19	0.541	0.131	0.266	51	0.003	2.656	0.084
20	0.097	0.127	0.111	52	0.005	3.519	0.129
21	0.244	0.041	0.1	63	0.071	0.172	0.111
22	3.375	0.24	0.901	65	0.034	0.018	0.025
23	0.473	0.561	0.515	66	0.132	0.165	0.148
24	1.304	0.237	0.557	67	0.029	0.02	0.024
25	0.261	0.184	0.219	68	0.009	0.006	0.008
26	1.106	0.117	0.359	69	0.02	0.007	0.012
27	0.216	0.045	0.099	70	0.016	0.003	0.007
28	0.919	0.065	0.245	71	0.011	0.006	0.008
29	0.027	0.021	0.024	72	0.004	0.001	0.002
30	1.032	0.069	0.267	80	0.001	5.3	0.055
31	0.24	0.073	0.132	81	0.001	5.527	0.069
32	1.21	0.118	0.379	82	0.001	5.585	0.074

Table S9. Contribution of each non-hydrogen atom to hole and electron in gCN-F.

Atom	Hole (%)	Electron (%)	Overlap	Atom	Hole (%)	Electron (%)	Overlap
1	12.677	0.993	3.549	33	0.323	0.256	0.287
2	2.186	2.685	2.423	34	0.152	0.195	0.172
3	8.97	0.773	2.634	35	0.294	0.045	0.115
4	1.759	3.132	2.347	36	1.694	0.278	0.687
5	0.227	5.289	1.095	37	0.631	0.686	0.658
6	2.477	1.983	2.216	38	4.877	0.308	1.225
7	8.412	2.781	4.836	39	0.757	0.163	0.351
8	1.82	7.422	3.676	40	2.035	0.072	0.383
9	8.732	2.914	5.044	41	0.409	0.048	0.139
10	1.847	3.748	2.632	42	1.516	0.043	0.256
11	9.457	0.88	2.886	43	0.198	0.687	0.369
12	2.206	3.037	2.589	44	0.042	0.034	0.038
13	11.833	1.28	3.892	45	0.03	0.042	0.036
14	0.172	0.692	0.345	46	0.093	11.105	1.018
15	0.234	7.164	1.294	47	0.024	4.614	0.332
16	1.191	0.038	0.212	48	0.009	3.319	0.17
17	0.319	0.038	0.11	49	0.003	2.334	0.083
18	1.578	0.077	0.349	50	0.005	4.863	0.151
19	0.496	0.135	0.258	51	0.003	2.545	0.086
20	0.085	0.132	0.106	52	0.004	3.416	0.112
21	0.229	0.04	0.096	63	0.069	0.202	0.118
22	3.064	0.252	0.879	65	0.021	0.021	0.021

23	0.434	0.584	0.503	66	0.108	0.196	0.146
24	1.158	0.245	0.533	67	0.018	0.023	0.021
25	0.232	0.189	0.209	68	0.006	0.007	0.006
26	0.965	0.118	0.337	69	0.009	0.008	0.008
27	0.195	0.048	0.096	70	0.006	0.003	0.004
28	0.862	0.065	0.237	71	0.008	0.008	0.008
29	0.02	0.022	0.021	72	0.004	0.002	0.003
30	1.121	0.075	0.29	77	0.001	4.949	0.051
31	0.257	0.079	0.143	78	0.001	5.184	0.068
32	1.282	0.128	0.405	79	0.001	5.247	0.064

11. References

1. W. B. Shao, R. S. Luo, J. Meng, X. K. Lv, H. M. Xiang, W. L. Xiao, X. Zhou, L. W. Liu, Z. B. Wu, S. Yang, *J. Agric. Food Chem*. **2023**, *71*, 16950–16961.

2. H. W. Liu, S. S. Su, S. Y. Ma, T. Li, W. Fang, Y. Ding, S. T. Liu, J. R. Zhang, H. M. Xiang, X. Zhou, S. Yang, *J. Agric. Food Chem*. **2023**, *71*, 11035-11047.

3. H. W. Wang, X. M. Tang, Y. C. Sun, Z. Huang, L. S. Zhao, *Chem. Eng. J.* **2024**, *480*, 148308.

4. Y. Feng, Y. Tao, J. H. Qu, Y. Zhang, *Chem. Eng. J.* **2023**, *472*, 145053.

5. H. Tu, Y. Xu, S. S. Chen, Y. Wang, S. X. Guo, J. Wu, *Adv. Energy Sustainability Res*. **2024**, 2400175.

6. R. D. Tang, D. X. Gong, Y. C. Deng, S. Xiong, J. F. Zheng, L. Li, Z. P. Zhou, L. Su, J. Zhao, *J. Hazard. Mater.* **2022**, *423*, 126944.

7. Y. Y. Fang, H. Y. Chen, T. Y. Sheng, S. Q. Lv, S. X. Cai, Y. Q. Liu, K. F. Zhang, *Sur. Interfaces* **2024**, *45*, 103848.